

# Chapter 6

## Multimode Solar-Pumped Lasers



Joana Almeida and Dawei Liang

Milestone multimode solar-pumped laser designs and their laser output performances are introduced in this chapter. Since the knowledge of imaging and nonimaging primary, secondary and tertiary concentrators are vital for successful solar laser designs, Zemax<sup>®</sup> and LASCAD<sup>™</sup> numerical analysis examples are provided in order to ensure student's clear understandings of how concentrated solar radiation is optically coupled and absorbed by the laser medium by Zemax<sup>®</sup> software and, consequently, how solar laser output power is numerically calculated by LASCAD<sup>™</sup> software.

### 6.1 Solar-Pumped Lasers with Imaging and Nonimaging Primary, Secondary and Tertiary Concentrators

The optical pumping of solar lasers relies on primary, secondary and tertiary concentrators to achieve enough pumping intensity for the lasing threshold [1–24]. These solar concentrators can be classified into two types: imaging and nonimaging, depending on whether the image of the sun is focused on the receiver or not [25]. The imaging and nonimaging concentrators responsible for the main advances in solar-pumped lasers will be addressed in the next sections.

#### 6.1.1 *Configurations for Solar Energy Collection and Concentration*

The Sun appears to move across the sky during the day due to the rotational motion of the Earth. The Sun's path across the sky also varies seasonally and with geographical location. The Earth's axial tilt of approximately  $23.5^\circ$  and its elliptical orbit around the Sun ensure that observers at different locations will see the apparent Sun motion

differently throughout the year [26]. For these reasons, solar systems (including solar-pumped lasers) require sun-tracking systems for the efficient capture of the solar radiation during the day and along the year. The solar energy collection by these systems can be done in two different ways: through direct tracking or indirect solar tracking by heliostat.

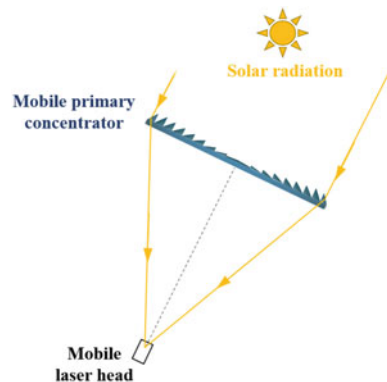
### 6.1.1.1 Direct Solar Tracking Type

In direct solar tracking systems, the primary concentrator and the receiver (the solar laser head in solar-pumped lasers) are both assembled to the solar tracker with their optical axes aligned with the position of the Sun in the sky, as illustrated in Fig. 6.1. This implicates that all the components of the laser system are movable.

In the early stages of solid-state solar lasers, direct solar tracking systems were adopted [1, 2]. In 1966, Young used an equatorial mount mechanism to support the first Neodymium (Nd): Yttrium Aluminum Garnet (YAG) solar laser system with a 0.61 m diameter paraboloidal mirror as primary concentrator [2]. The equatorial tracking, also known as polar or spinning-elevation tracking, is commonly used in telescopes, where the principal axis—the polar axis—is always oriented towards the North Star, by which the Earth's axis of rotation is oriented. Therefore, this axis tracks the Sun in East–West direction. A secondary axis, named as declination axis and perpendicular to the polar axis, is also needed to correct the solar declination angle that changes along the year, tracking the Sun in North–South direction [27, 28].

Between the middle 1980s and early 2000s, solar laser systems with stationary focus have gained strength with the use of large size mirrors as primary concentrators, for which heliostats were required to redirect the solar radiation towards the static laser head [3–8]. Nevertheless, as of 2007, direct solar tracking systems were employed again in solar-pumped lasers with the adoption of the economically competitive Fresnel lenses as primary concentrators [9–14]. The low weight of the Fresnel lenses facilitated their assembly on solar trackers, allowing the development of much lighter and more compact solar laser systems and avoiding additional power

**Fig. 6.1** Direct solar energy collection and concentration configuration



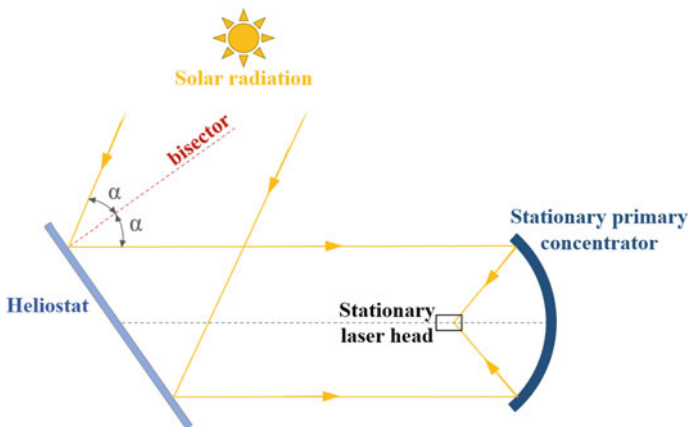
losses with the use of heliostats. Moreover, unlike the reflective concentrators, the focal spot of Fresnel lenses lies in their rear side. Consequently, the laser head along with the laser resonator and mechanical support are positioned behind the Fresnel lens, as shown in Fig. 6.1, enabling its easy access during the experiments.

### 6.1.1.2 Heliostat Type

A Heliostat, from *helios* (the Greek word for Sun) and *stat* (stationary), is a device composed of one or more mirrors that redirects the solar radiation towards a static receiver [29]. The mirrored surface of the heliostat is kept perpendicular to the bisector of the angle between the Sun's position in the sky and the stationary receiver, as illustrated in Fig. 6.2.

The conventional heliostat configuration is based on the variation of two axes simultaneously [30]: The azimuth axis and the elevation axis. The azimuth axis is vertical relative to the heliostat base, tracking the angle bisector between the Sun and the receiver in the East–West direction. The elevation (or altitude) axis is normal to the azimuth axis, tracking the Sun in North–South direction. The configuration azimuth-elevation is also used in direct solar tracking systems with Fresnel lenses, with the azimuth axis tracking the Sun position [13].

Heliostats began to be implemented in solar laser systems in the mid-1980s [3, 4]. In order to reach higher solar laser output power levels, large size mirror concentrators were used to pump the laser medium, for which direct solar tracking became inappropriate. The attachment of heavy solar laser systems on a solar tracker structure would lead to higher energy requirements for tracking [27]. Besides, the focusing method of reflective concentrators requires the receiver to be placed in their front (Fig. 6.2), which would make the direct tracking even more troublesome, especially



**Fig. 6.2** Indirect solar energy collection and concentration configuration via heliostat

in the daily hours of greatest solar irradiance when the Sun reaches its highest position in the sky, obliging the receiver to be located above the primary concentrator. Therefore, heliostats were needful to redirect the solar radiation towards the laser head [3–8].

Despite the progress in solar laser collection efficiency that led to a reduction in primary mirror concentrator area, heliostats are still used in solar laser systems with reflective concentrators, guaranteeing steady solar laser head within the laboratory [15–22, 24].

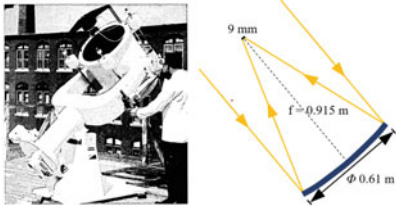
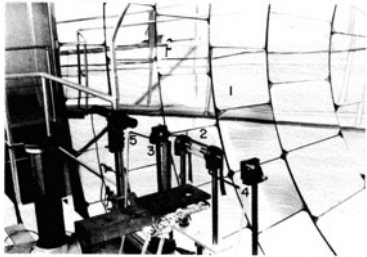
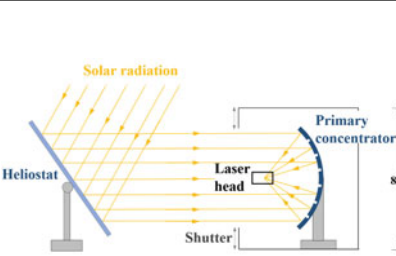
### ***6.1.2 Parabolic Mirrors and Fresnel Lens as Primary Imaging Concentrators***

Solar pumping of lasers requires primary concentrators with high concentration ratios to obtain sufficient gain in the irradiated active medium.

Primary mirror concentrators of paraboloidal shape have long been exploited by solar laser researchers to stimulate the laser medium, as summarized in Table 6.1. In 1966, Young used a  $\varnothing$  0.61 m aluminized parabolic mirror to pump the first Nd:YAG solar laser of 1 W in continuous wave (cw) mode [2]. Between the mid and late 1980s, large-size stationary mirror concentrators with apertures up to 10 m were adopted as primary concentrators [3, 4]. This permitted obtaining high solar powers at the focus and cw laser output power levels of more than 60 W [4]. The highest solar laser output power of 500 W cw was further achieved in 1993 by Krupkin et al. [6] using 64 paraboloidal mirrors in the heliostat field of Weizmann Institute (WIS) Solar Tower with total collection area of 660 m<sup>2</sup>. Nevertheless, the solar laser collection efficiency (the laser output power per unit of primary concentrator area) was only 0.76 W/m<sup>2</sup> [7]. Besides, the solar tower configuration has the drawback of causing astigmatic aberration and focal spot increase [31]. To overcome this problem, Lando and his co-workers built an Astigmatic Corrected Target Aligned (ACTA) solar concentrator [31]. In this device, a segmented primary mirror with 3.4 m aperture was mounted on a two-axis positioner which tracked the solar orbit. The primary concentrator focused the incoming solar radiation towards a plane folding mirror, which in turn deflected the light towards the stationary solar laser head within an enclosure, as shown in Table 6.1. Through this collection and concentration system, with primary concentrator aperture much smaller than the previous ones [3, 4, 6], 6.7 W/m<sup>2</sup> collection efficiency was reached, constituting a substantial progress in solar laser efficiency at that decade [7]. Since the work of Lando et al. [7], solar laser researchers started to pay more attention to the solar laser efficiency rather than the laser output power for the assessment of the solar laser performance [9–23].

Significant progress in solar laser collection efficiency and reduction in the collection area have occurred with the adoption of Fresnel lenses as primary concentrators in direct solar tracking systems, as summarized in Table 6.2. Solar laser collection efficiency of 32.1 W/m<sup>2</sup> with Fresnel lens system was reached in 2018 by Guan


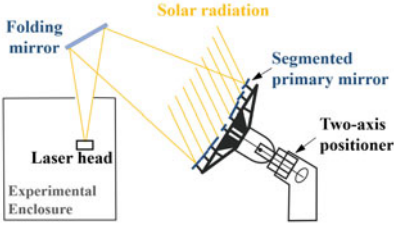
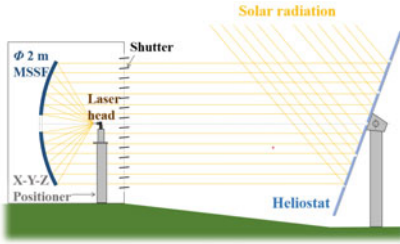
**Table 6.1** Solar collection and concentration systems of milestone solar lasers with primary mirror concentrators

Year	Authors [Ref.]	Milestones
Primary concentrator (image) Place		Parameters
1966	Young [2]	First 1 W cw Nd:YAG solar laser
	American Optical Company, USA	<p>Solar tracking: Direct</p> <p><b>Primary concentrator: Parabolic mirror</b>                      Diameter: 0.61 m                      Full collection area: ~0.293 m<sup>2</sup>                      Focal length: 0.915 m                      Focal spot diameter: ~9 mm                      Reflectivity: 85%</p>
1984	Arashi et al. [3]	18 W cw solar laser power
	1. Parabolic mirror; 2. Nd-YAG laser head; 3. High reflection mirror; 4. Output mirror; 5. He-Ne laser for optical alignment Tohoku University (TU), Japan	<p>Solar tracking: Heliostats (Segmented flat mirror)</p> <p><b>Primary concentrator: Segmented paraboloidal mirror [3]</b>                      Diameter: 10 m                      Full collection area: ~78.5 m<sup>2</sup>                      Focal length: 3.2 m                      Rim-angle: 76° [33]                      FWHM<sup>1</sup> focal spot: ~40 mm                      Maximum power at the focus: 55 kW</p> <p><b>Effective solar power for pumping: 1.1 kW</b>  <b>Effective collection area: ~13.1 m<sup>2</sup></b></p>
1988	Weksler and Schwartz [4]	> 60 W cw solar laser power
	Weizmann Institute of Science (WIS), Israel	<p>Solar tracking: Heliostats (10×10 m<sup>2</sup> segmented flat mirror)</p> <p><b>Primary concentrator: Segmented mirror made of 600 small spherical mirrors</b>                      Diameter: 7.3 m [34]                      Full collection area: ~38.5 m<sup>2</sup> [7]                      Focal length: 3.5 m                      Rim-angle: 65° [34]                      FWHM focal spot: ~40 mm                      Maximum power: &gt;15 kW</p> <p><b>Effective solar power for pumping: ~5 kW</b>  <b>Effective collection area: ~12.8 m<sup>2</sup></b></p>

<sup>1</sup> FWHM—Full Width at Half Maximum.

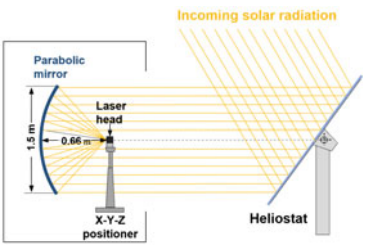
(continued)

**Table 6.1** (continued)

<p><b>1993</b></p>	<p>Krupkin et al. [6]</p>	<p>500 W cw solar laser power</p>
 <p style="text-align: center;">WIS, Israel</p>		<p>Solar tracking: Heliostats</p> <p><b>Primary concentrator: Heliostat parabolic mirrors field</b> [6]                  Full collection area: 3500 m<sup>2</sup> [6]                  Maximum power: ~2.8 MW [35]  <b>Effective collection area: ~660 m<sup>2</sup></b> [7]</p>
<p><b>2003</b></p>	<p>Lando et al. [7]</p>	<p>6.7 W/m<sup>2</sup> solar laser collection efficiency</p>
 <p style="text-align: center;">WIS, Israel</p>		<p>Solar tracking: ACTA solar concentrator</p> <p><b>Primary concentrator: Segmented mirror</b> composed of 61 hexagonal mirrors spherically curved                  Diameter: 3.4 m                  Full collection area: 6.85 m<sup>2</sup>                  Focal length: 8.5 m  <b>Effective collection area: 6.75 m<sup>2</sup></b></p>
<p><b>2012</b></p>	<p>Almeida et al. [23]</p>	<p>0.29 W multimode laser beam brightness</p>
<p><b>2017</b></p>	<p>Liang et al. [17]</p>	<p>31.5 W/m<sup>2</sup> solar laser collection efficiency                  5.25% slope efficiency</p>
 <p style="text-align: center;">PROMES-CNRS, France</p>		<p>Solar tracking: Heliostat (Flat mirror with 36 segments of 0.5×0.5 m<sup>2</sup> each)</p> <p><b>Primary concentrator: Parabolic mirror</b>                  Diameter: 2.0 m;                  Full collection area: ~3.07 m<sup>2</sup>                  Focal length: 0.85 m                  Rim-angle: 60°                  FWHM focal spot: ~10 mm [36]                  Maximum power: ~2 kW [36]                  Combined reflectivity (heliostat plus parabolic mirror): 59%  <b>Effective collection areas: 2.88 m<sup>2</sup></b> [23] 1.18 m<sup>2</sup> [17]</p>
<p><b>2018</b></p>	<p>Liang et al. [21]</p>	<p>32.5 W/m<sup>2</sup> Cr:Nd:YAG solar laser collection efficiency                  6.7% slope efficiency</p>
<p><b>2019</b></p>	<p>Liang et al. [15]</p>	<p>Side-pumped solar laser with 5.4% slope efficiency</p>

(continued)

**Table 6.1** (continued)



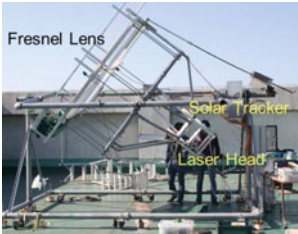
<b>2020</b>	Liang et al. [18]	Simultaneous solar laser emissions from three Nd:YAG rods
<b>2021</b>	Vistas et al. [16]	Ce:Nd:YAG side-pumped solar laser with 23.6 W/m <sup>2</sup> collection efficiency
<b>2022</b>	García et al. [19]	Single-rod Ce:Nd:YAG solar laser with 4.5% conversion efficiency Lowest threshold solar power
<b>2022</b>	Liang et al. [20]	Most efficient simultaneous emissions from three Ce:Nd:YAG laser rods 4.64% solar-to-laser conversion efficiency 41.3 W/m <sup>2</sup> solar laser collection efficiency 7.64% slope efficiency
 <p data-bbox="182 820 523 873">NOVA School of Science and Technology (FCT NOVA), Portugal</p>		<p data-bbox="570 590 940 643">Solar tracking: Heliostat (Flat mirror with two segments)</p> <p data-bbox="570 652 917 679"><b>Primary concentrator: Parabolic mirror</b></p> <p data-bbox="570 679 705 702">Diameter: 1.5 m</p> <p data-bbox="570 702 805 725">Full collection area: 1.767 m<sup>2</sup></p> <p data-bbox="570 725 735 747">Focal length: 0.66 m</p> <p data-bbox="570 747 693 770">Rim-angle: 60°</p> <p data-bbox="570 770 787 793">Maximum power: ~1.2 kW</p> <p data-bbox="570 793 987 816">Combined reflectivity (heliostat plus parabolic mirror): 75%</p> <p data-bbox="570 855 1017 908"><b>Effective collection areas:</b> 1.0 m<sup>2</sup> [21]; 0.9 m<sup>2</sup> [15]; 1.0 m<sup>2</sup> [18]; 0.7 m<sup>2</sup> [16]; 0.29 m<sup>2</sup> [19]; 0.4 m<sup>2</sup> [20]</p>

Images adapted from [2–4, 7, 21, 24, 32]

et al. using an effective collection area of only 1.03 m<sup>2</sup> to end-side-pump a bonding Nd:YAG/YAG laser rod [14].

Compared with parabolic mirror systems, Fresnel lens systems reduce complexity, weight, and cost of solar lasers. However, they have chromatic aberration, i.e., spreading the solar radiation spectrum along its focal zone, which may impair the transfer efficiency of the pump radiation to the laser medium. Parabolic mirrors, instead, collect all pumping wavelengths to a small focal spot without dispersion. For these reasons, the solar laser researchers from FCT NOVA have insisted on enhancing the solar laser efficiency using parabolic mirror as primary concentrators. Since 2017, several important milestone solar lasers occurred at the solar facilities of FCT NOVA and PROMES-CNRS (Table 6.1), both composed of an heliostat and a stationary parabolic mirror with 1.5 and 2.0 m maximum diameter, respectively [15–21, 37]. Records in solar-to-laser conversion, collection, and slope efficiencies of 4.64%, 41.3 W/m<sup>2</sup>, and 7.64% were, respectively, attained in 2022 by the simultaneous end-side-pumping of three Cerium (Ce):Nd:YAG laser rods through the NOVA solar facility [20].

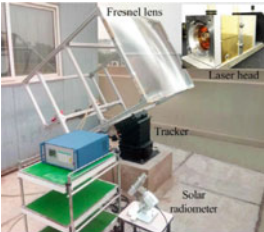
**Table 6.2** Solar collection and concentration systems of milestone solar lasers with primary Fresnel lens concentrators

Year	Authors [Ref.]	Milestones
Primary concentrator (image) Place		Parameters
2007	Yabe et al. [9]	18.7 W/m <sup>2</sup> solar laser collection efficiency with Cr:Nd:YAG active medium
 <p>Tokyo Institute of Technology (TIT), Japan</p>		<p>Solar tracking: Direct</p> <p><b>Primary concentrator: Fresnel lens</b>                      Aperture: 1.4×1.05 m<sup>2</sup>                      Focal length: 1.2 m                      FWHM focal spot: 11.2 mm                      Transmission: 66.4%</p> <p><b>Effective solar power for pumping: ~865 W</b>  <b>Effective solar collection area: ~1.3 m<sup>2</sup></b></p>
2011	Liang and Almeida [13]	19.3 W/m <sup>2</sup> solar laser collection efficiency with Nd:YAG active medium
 <p>FCT NOVA, Portugal</p>		<p>Solar tracking: Direct</p> <p><b>Primary concentrator: Fresnel lens</b>                      Diameter: 0.9 m                      Focal length: 1.2 m                      FWHM focal spot: ~12 mm                      Transmission: 78.6%</p> <p><b>Effective solar power for pumping: ~445 W</b>  <b>Effective solar collection area: 0.636 m<sup>2</sup></b></p>
2012	Dinh et al. [10]	30 W/m <sup>2</sup> solar laser collection efficiency
 <p>TIT, Japan</p>		<p>Solar tracking: Direct</p> <p><b>Primary concentrator: Fresnel lens</b>                      Aperture: 2×2 m<sup>2</sup>                      Focal length: 2 m                      FWHM focal spot: ~20.4 mm<sup>[11]</sup>                      Transmission: 50%</p> <p><b>Effective solar power for pumping: 1840 W</b>  <b>Effective solar collection area: 4 m<sup>2</sup></b></p>

(continued)



**Table 6.2** (continued)

<p><b>2018</b></p>	<p>Guan et al. [14]</p>	<p>32.1 W/m<sup>2</sup> Nd:YAG solar laser collection efficiency</p>
 <p>Beijing Institute of Technology (BIT), China</p>		<p>Solar tracking: Direct</p> <p><b>Primary concentrator: Fresnel lens</b>                  Aperture: 1.4×1.05 m<sup>2</sup>                  Focal length: 1.2 m                  FWHM focal spot: 11.5 mm</p> <p><b>Effective solar collection area: 1.03 m<sup>2</sup></b></p>

Images adapted from [9, 11, 13, 14]

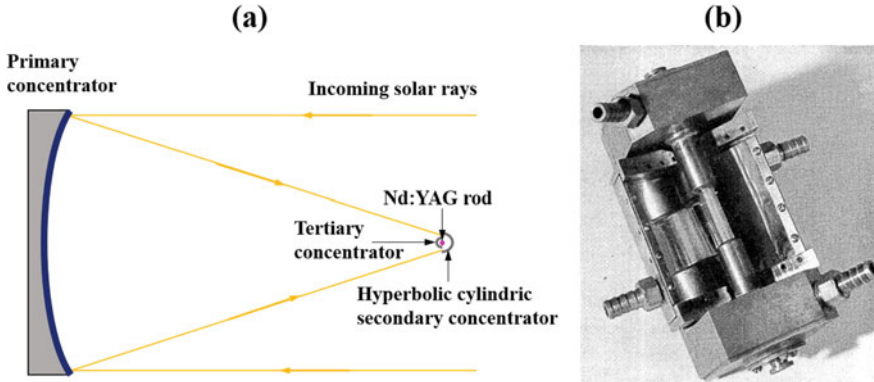
### 6.1.3 Secondary Imaging Concentrators

The concentrated solar intensity of the primary concentrator is limited by the Sun image at the focus, which can lead to a significant mismatch between the sizes of the focal spot and the laser active medium. Thence, for efficient coupling of the solar rays into the laser medium, the focal image must be reduced, which requires secondary optics. In this section, the secondary imaging concentrators that contributed to the most significant advances in solar lasers are presented.

#### 6.1.3.1 Hyperbolic-Cylindrical Reflector for Side-Pumping Scheme

The first 1 W cw Nd:YAG solar laser was pumped through a modified Cassegrain sun-tracking telescope consisting of a 0.61 m diameter paraboloidal primary mirror, a water-cooled hyperbolic-cylindric secondary mirror and a hemicircular cylindric tertiary mirror, as shown in Fig. 6.3 [2]. The aluminized secondary concentrator, as well as the primary concentrator, had an average reflection of 85% in the pump bands.

In this solar laser system, a side-pumping configuration was adopted, which means that the solar radiation was injected into the laser medium transversely to its optical axis. Thus, to refocus and redistribute the concentrated solar radiation along the 3 mm diameter, 30 mm length, 1.0 at.% Nd:YAG rod, both secondary and tertiary concentrators were two-dimensional. The resultant image at the focus of the hyperbolic-cylindric reflector was 3 mm by 24 mm, which was coincident with the exposed portion of the active medium [2]. The laser resonator was formed by the highly and partially reflective coatings in the laser emission wavelength (1064 nm) deposited on the convex end surfaces of laser rod with 5 cm radius of curvature [2].



**Fig. 6.3** a Schematic design of the 1 W cw Nd:YAG solar laser system (adapted from [2]) b Assembly of the hyperbolic-cylindrical secondary concentrator [2]

### 6.1.3.2 Meniscus Plus Hyper Hemispherical Aplanatic Refractors for End-Side-Pumping Scheme

An aplanatic lens is free of both spherical and coma aberrations, being widely used in microscope objectives. They are usually made of at least two or three air-spaced lens elements [38].

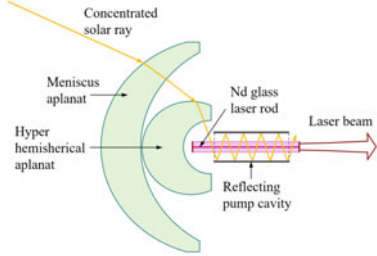
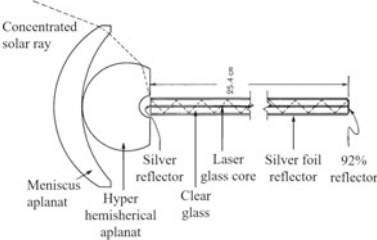
In 1964 and 1966, Simpson [1] and Young [2] utilized this type of lenses as secondary concentrators in their solar laser experiments with Nd:glass medium, combining a meniscus converging lens with a hyper hemispherical lens to pump the laser rod, as shown in Table 6.3. A meniscus converging lens is a convex-concave lens thicker at the center than at the edges, being free from both spherical and coma aberrations [39]. When combined with the hyper hemispherical lens, which has a very wide field of view angle [40], the focal length of the solar laser system is shortened and, consequently, the focal spot is reduced. With this configuration, the more external solar rays could ricochet along the rod, allowing multipass pumping to the thin laser rod.

Young succeeded in obtaining Nd:glass solar laser output power of 1.25 W [2]. However, no provisions were made to cool the laser rod in both experiments [1, 2]. Therefore, laser operation lasted less than 1.0 s before cessation owing to excessive temperature.

### 6.1.3.3 Fused Silica Aspheric Lens for Both End- and Side-Pumping Schemes

Aspherical lenses encompass any lens with rotational symmetry that has a non-spherical surface, in which the radius of curvature varies radially from the center to the edge. These lenses can focus all the incident light on the same focal region,

**Table 6.3** Milestone solar lasers with meniscus plus hyper hemispherical aplanat refractors as secondary concentrators

Year	Authors [Ref.]	Milestones
Secondary concentrator (image)		Solar laser system parameters
<b>1964</b>	Simpson [1]	First Nd:glass solar laser
		<p>Primary concentrator: 0.61 m diameter Parabolic mirror</p> <p><b>Secondary concentrator: Meniscus plus hyper hemispherical aplanats</b> SF-4 glass material</p> <p>Tertiary concentrator: Silvered reflector</p> <p>Active medium: Ø 0.1 mm × 30 mm Nd-doped barium crown glass core clad by Ø 1.0 mm soda-lime silicate glass</p>
<b>1966</b>	Young [2]	1.25 W Nd:glass solar laser
		<p>Primary concentrator: 0.61 m diameter Parabolic mirror</p> <p><b>Secondary concentrator: Meniscus plus hyper hemispherical aplanats</b> SF-4 glass material</p> <p>Tertiary concentrator: Silver foil reflector</p> <p>Active medium: Ø 0.4 mm Nd:glass core clad by Ø 4.0 mm clear glass</p>

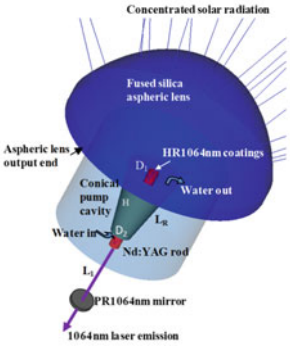
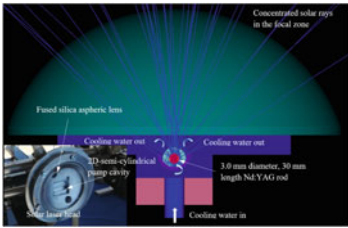
Images adapted from [1] and [2], respectively

reducing spherical aberration and providing true diffraction-limited spot sizes. The concentrated solar radiation can hence be collected and compressed efficiently from the focal zone of the primary concentrator into the laser medium. For these reasons, fused silica aspherical lenses have been used as secondary concentrators in several solar-pumped laser systems with either side-pumping or end-side-pumping configurations [15–20], summarized in Table 6.4. Fused silica material is suitable for solar-powered lasers since it has a wide transparency range over the laser media absorption spectra. Furthermore, it is very resistant to high temperature and thermal shock [41].

The curvature surface of the aspheric lenses ( $z$ ) utilized in these solar laser systems followed Eq. (6.1) [19]:

$$z = \frac{RoCr^2}{1 + \sqrt{1 - (1 + k)RoC^2r^2}} + \alpha_1 r^2 \tag{6.1}$$

**Table 6.4** Milestone solar lasers with aspherical lenses as secondary concentrators

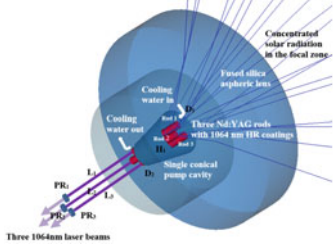
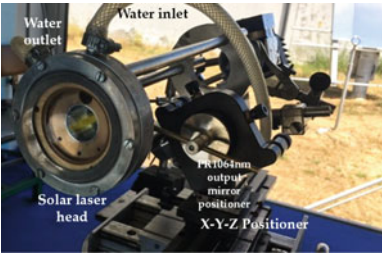
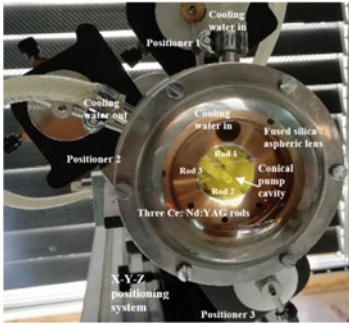
Year	Authors [Ref.]	Milestones
Secondary concentrator (image) <b>Laser head configuration</b>		Solar laser system parameters
<b>2017</b>	Liang et al. [17]	31.5 W/m <sup>2</sup> collection efficiency 5.25% slope efficiency
 <p style="text-align: center;"><b>End-side-pumping</b></p>		<p>Primary Concentrator, effective collection area: PROMES-CNRS parabolic mirror, 1.18 m<sup>2</sup></p> <p><b>Secondary concentrator: Aspheric Lens</b>                      Radius of curvature <math>RoC</math>: 45 mm                      Flat output surface                      Radial aperture <math>r</math>: 42 mm                      Conic constant <math>k</math>: 0                      Height: 38 mm                      Aspheric coefficient <math>\alpha_1</math>: -0.005</p> <p>Tertiary concentrator: Conical reflector                      Active medium: <math>\varnothing</math> 4 mm <math>\times</math> 35 mm Nd:YAG</p>
<b>2019</b>	Liang et al. [15]	Side-pumped Nd:YAG solar laser with 5.4% slope efficiency
 <p style="text-align: center;"><b>Side-pumping</b></p>		<p>Primary Concentrator, effective collection area: FCT NOVA parabolic mirror, 0.9 m<sup>2</sup></p> <p><b>Secondary concentrator: Aspheric Lens</b>                      Radius of curvature <math>RoC</math>: 44 mm                      Flat output surface                      Radial aperture <math>r</math>: 40 mm                      Conic constant <math>k</math>: 0                      Height: 31 mm                      Aspheric coefficient <math>\alpha_1</math>: -0.002</p> <p>Tertiary concentrator: Semi-cylindrical reflector                      Active medium: <math>\varnothing</math> 3 mm <math>\times</math> 30 mm Nd:YAG</p>

(continued)

where  $RoC$  is the radius of curvature,  $r$  is the radial aperture,  $k$  the conic constant, and  $\alpha_1$  the aspheric coefficient.

The most efficient Nd:YAG solar laser with parabolic mirror as primary concentrator was obtained with the use of a secondary aspherical lens in an end-side-pumping scheme [17]. In end-side-pumping configurations, most of the concentrated solar radiation is directly focused onto the end face of the laser rod, i.e., parallel to the laser beam. Therefore, the optical path of solar rays within the laser medium is much longer than that of side-pumping scheme, enabling higher pumping efficiency.

**Table 6.4** (continued)

<p><b>2020</b></p>	<p>Liang et al. [18]</p>	<p>First simultaneous solar laser emissions from three Nd:YAG rods</p>
 <p><b>End-side-pumping</b></p>	<p>Primary Concentrator, effective collection area: FCT NOVA parabolic mirror, 1.0 m<sup>2</sup></p> <p><b>Secondary concentrator: Aspheric Lens</b>              Radius of curvature <i>RoC</i>: 60 mm              Flat output surface              Radial aperture <i>r</i>: 42 mm              Conic constant <i>k</i>: 0              Height: 34 mm              Aspheric coefficient <math>\alpha_1</math>: -0.003</p> <p>Tertiary concentrator: Conical reflector</p> <p>Active medium: Three <math>\varnothing</math> 3.0 mm <math>\times</math> 25 mm Nd:YAG</p>	
<p><b>2022</b></p>	<p>Garcia et al. [19]</p>	<p>Single-rod Ce:Nd:YAG solar laser with 4.5% conversion efficiency              Lowest threshold solar power</p>
 <p><b>End-side-pumping</b></p>	<p>Primary Concentrator, effective collection area: FCT NOVA parabolic mirror, 0.293 m<sup>2</sup></p> <p><b>Secondary concentrator: Aspheric Lens</b>              Radius of curvature <i>RoC</i>: 43 mm              Flat output surface              Radial aperture <i>r</i>: 41 mm              Conic constant <i>k</i>: 0              Height: 37 mm              Aspheric coefficient <math>\alpha_1</math>: -0.004</p> <p>Tertiary concentrator: Conical reflector</p> <p>Active medium: <math>\varnothing</math> 2.5 mm <math>\times</math> 25 mm Ce:Nd:YAG</p>	
<p><b>2022</b></p>	<p>Liang et al. [20]</p>	<p>Most efficient simultaneous emissions from three Ce:Nd:YAG laser rods              4.64% solar-to-laser conversion efficiency              41.3 W/m<sup>2</sup> solar laser collection efficiency              7.64% slope efficiency</p>
 <p><b>End-side-pumping</b></p>	<p>Primary Concentrator, effective collection area: FCT NOVA parabolic mirror, 0.4 m<sup>2</sup></p> <p><b>Secondary concentrator: Aspheric Lens</b>              Radius of curvature <i>RoC</i>: 43 mm              Flat output surface              Radial aperture <i>r</i>: 42 mm              Conic constant <i>k</i>: 0              Height: 37 mm              Aspheric coefficient <math>\alpha_1</math>: -0.005</p> <p>Tertiary concentrator: Conical reflector</p> <p>Active medium: Three <math>\varnothing</math> 2.5 mm <math>\times</math> 25 mm Ce:Nd:YAG</p>	

Images adapted from [15, 17–20]

Nevertheless, end-side-pumping can lead to severe thermal loading issues in single solid-state laser media of cylindrical geometry [42, 43], due to the non-homogenous pumping light distribution along the laser rod's length, precluding these laser systems to scale to high power. To attenuate this drawback, the potential of multirod solar laser systems based on the simultaneous pumping of several laser media has been recently investigated [18, 20]. In these systems, each rod absorbs only a portion of the concentrated solar radiation incident on the pumping cavity, reducing significantly the thermal induced effects. The records in solar-to-laser conversion, collection, and slope efficiencies of 4.64%, 41.3 W/m<sup>2</sup>, and 7.64%, respectively, were attained through the simultaneous pumping of three Ce:Nd:YAG laser rods using an aspherical lens as secondary concentrator (Table 6.4) [20].

Side-pumping configuration is also suitable for laser power scaling once it spreads the solar radiation along the laser rod, hence improving the thermal performance. The most efficient side-pumped Nd:YAG solar laser with 2.43% solar-to-laser power conversion efficiency, 17.7 W/m<sup>2</sup> collection efficiency and 5.4% slope efficiency had also an aspheric lens as secondary concentrator (Table 6.4) [15].

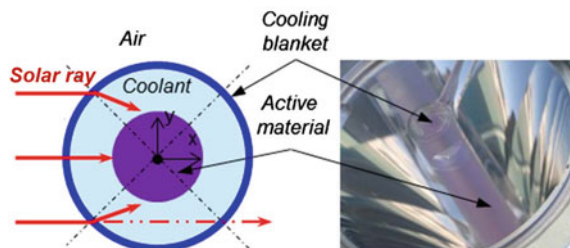
#### 6.1.3.4 Liquid Light Guide Lens for End-Side-Pumping Scheme

The liquid light guide lens can be considered as a laser flow tube. Nonetheless, it can also work as a lens due to the difference of refraction index  $n$  between the air ( $n_{air} = 1$ ) and the coolant (usually water,  $n_{water} = 1.33$ ), as shown in Fig. 6.4.

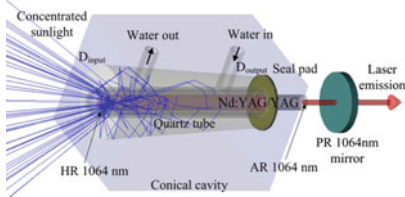
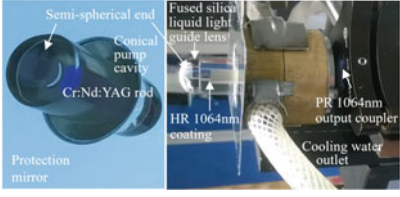
In 2012, Dinh and his co-workers utilized a liquid light guide lens to improve the performance of an end-side-pumping solar laser system, composed of a Fresnel lens primary concentrator and a secondary conical mirror (Fig. 6.4) [10, 11]. In this case, the liquid light guide lens worked essentially as a tertiary concentrator, helping to refocus the reflected solar rays by the conical cavity into the laser rod. With this configuration, 120 W cw laser power was produced from a 6 mm diameter, 100 mm length Nd:YAG rod, resulting in 30 W/m<sup>2</sup> collection efficiency. Such result was 2 times higher than that without the glass tube, i.e., with the conical cavity flooded with water [10, 11].

In 2018, Guan et al. [14] and Liang et al. [21] developed liquid light guide lenses with hemispherical front surfaces to end-side-pump a bonding Nd:YAG/YAG [14] and a Cr:Nd:YAG rod [21], respectively, within a conical cavity. The curved front

**Fig. 6.4** Liquid light guide lens configuration. Adapted from [11]



**Table 6.5** Milestone solar lasers with liquid light guide lens as secondary concentrators

Year	Authors [Ref.]	Milestones
Secondary concentrator (image)		Solar laser system parameters
2018	Guan et al. [14]	<p>32.1 W/m<sup>2</sup> Nd:YAG/YAG solar laser collection efficiency</p>  <p>Primary Concentrator, effective collection area: BIT Fresnel lens, 1.03 m<sup>2</sup></p> <p><b>Secondary concentrator: Liquid light guide lens</b>                      Material: quartz                      Hemispherical input surface; <i>RoC</i>: 6 mm                      External/internal diameters: 12 mm / 10mm                      Length: 81 mm</p> <p>Tertiary concentrator: Conical reflector                      Active medium: Ø 6 mm × 95 mm bonding Nd:YAG/YAG</p>
2018	Liang et al. [21]	<p>32.5 W/m<sup>2</sup> Cr:Nd:YAG solar laser collection efficiency                      6.7% slope efficiency</p>  <p>Primary Concentrator, effective collection area: FCT NOVA parabolic mirror, 1.0 m<sup>2</sup></p> <p><b>Secondary concentrator: Liquid light guide lens</b>                      Material: Fused silica                      Hemispherical front surface; <i>RoC</i>: 8.5 mm                      Flat output surface</p> <p>Tertiary concentrator: Conical reflector                      Active medium: Ø 4.5 mm × 35 mm Cr:Nd:YAG</p>

Images adapted from [14] and [21], respectively

surface allowed the concentrated solar rays to be more efficiently focused on the top region of the laser rod, so the light guide lens acted as a secondary concentrator. These pumping configurations led to the records in solar laser collection efficiencies of 32.1 and 32.5 W/m<sup>2</sup> with Nd:YAG [14] and Cr:Nd:YAG laser materials [21], respectively, as summarized in Table 6.5. Similar configuration with liquid light guide lens as a secondary concentrator was also adopted for the first Ce:Nd:YAG solar laser [22].

### 6.1.4 Secondary Nonimaging Concentrators

Nonimaging concentrators can be considered as a funnel for light, sacrificing the image of the source in order to concentrate the light to intensities approaching the

theoretical limit [44]. They have played an important role in the advancement of solar-pumped lasers, acting as secondary and/or tertiary concentrators. In this section, the secondary nonimaging concentrators that contributed to the most significant advances in solar lasers are presented.

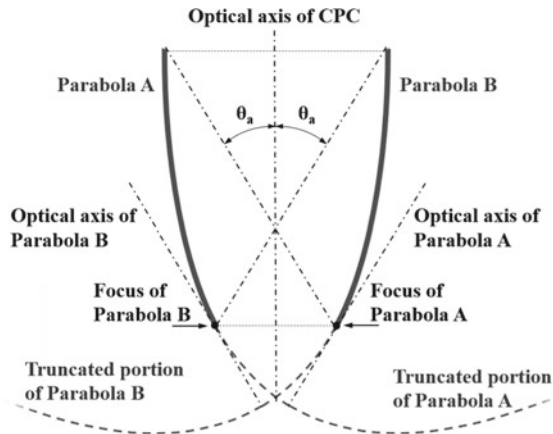
#### 6.1.4.1 Three-Dimensional Compound Parabolic Concentrator (3D-CPC) for Side-Pumping Scheme

One of the most representative nonimaging type concentrators is the compound parabolic concentrator (CPC), also known as Winston-type collector [45]. The three-dimensional (3D) CPC shape is derived from the CPC design principle for a flat receiver, represented in Fig. 6.5. It is based on the intersection of two parabolas facing each other, the axes of which are inclined at angles  $\pm \theta_a$  with respect to optical axis of the collector. The angle  $\theta_a$  is the acceptance angle of the concentrator, i.e., the angle at which the incoming sunlight can be captured by a concentrator and reflected to the absorber. Because of the CPC shape, all the incident solar rays within the maximum concentration angle  $\theta_a$  can be transmitted to a small output aperture emitting into a larger angle. This implies that irradiance is larger at the output aperture than at the entrance aperture, leading to a net concentration of the pump radiation [46].

The use of secondary 3D-CPCs concentrators has contributed to the advances of solar lasers in the 90's and early 2000s [6, 7], as summarized in Table 6.6.

In 2003, Lando et al. reached  $6.7 \text{ W/m}^2$  by using a 3D-CPC combined with a 2D-CPC tertiary concentrator to side-pump a Nd:YAG laser rod [7]. Similar archetype has been previously utilized by Krupkin et al. in 1993 to side-pump an array of laser rods at the WIS solar tower, reaching 500 W cw solar laser power [6].

**Fig. 6.5** Schematic design of a compound parabolic concentrator (CPC) for a flat receiver





**Table 6.6** Milestone solar lasers with secondary three-dimensional compound parabolic concentrators (3D-CPCs)

Year	Authors <sup>[Ref.]</sup>	Milestones
Secondary concentrator (image)		Solar laser system parameters
1993	Krupkin <i>et al</i> <sup>[6]</sup>	500 W Nd:YAG solar laser power
		Primary concentrator, effective collection area: WIS heliostat parabolic mirrors, 660 m <sup>2</sup> <b>Secondary concentrator: 3D-CPC</b> Tertiary concentrator: 2D-CPC Active medium: Array of laser rods
2003	Lando <i>et al</i> <sup>[7]</sup>	6.7 W/m <sup>2</sup> Nd:YAG solar laser collection efficiency
		Primary concentrator, effective collection area: WIS ACTA solar concentrator, 6.75 m <sup>2</sup> <b>Secondary concentrator: 3D-CPC</b> Input aperture: 100 mm Output aperture: 24 mm Maximum output half angle: 55° Tertiary concentrator: 2D-CPC Active medium: Ø 6.0 mm × 72 mm Nd:YAG

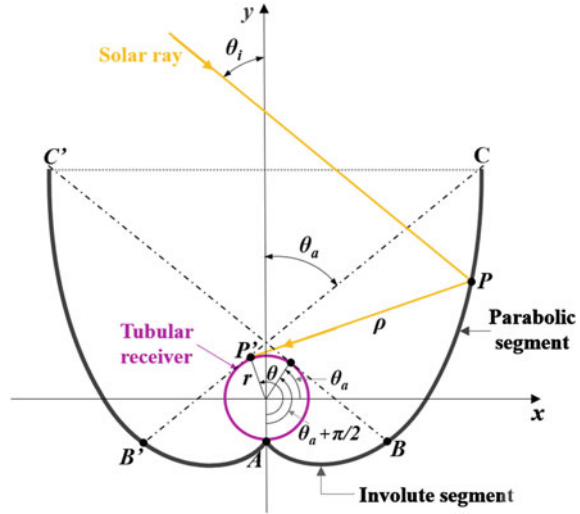
Images adapted from [6] and [7], respectively

### 6.1.4.2 Two-Dimensional Compound Parabolic Concentrator (2D-CPC) for Side-Pumping

The CPC can take a variety of shapes depending on the receiver geometry [47]. For solar-pumped lasers, the classical two-dimensional (2D) CPC profile is based on the design principle for tubular receivers, illustrated in Fig. 6.6. This CPC type has two different segments that smoothly join at point  $B(B')$  related to  $\theta_a$ . The lower segment, from the bottom of the receiver,  $A$ , to point  $B(B')$  is an involute of the receiver's cylindrical cross-section. The upper segment, from point  $B(B')$  to  $C(C')$ , is of parabolic shape.

A light ray entering the 2D-CPC with an angle  $\theta_i = \theta_a$  will strike the tubular receiver of radius  $r$  tangentially. The distance along the tangent from the receiver ( $P'$ ) to the last intersection point of the ray with the concentrator ( $P$ ) is represented by  $\rho$ , which is given by the following equation for the two CPC segments [48], where  $\theta$  is the angle between the radius to the bottom of the receiver and the radius to the tangential point  $P'$ :

**Fig. 6.6** Cross-section of a two-dimensional compound parabolic concentrator (2D-CPC) classical design for a tubular absorber. Adapted from [48]



$$\rho = \begin{cases} r\theta & \text{if } |\theta| \leq \theta_a + \pi/2 \\ r \left[ \frac{\theta + \theta_a + \pi/2 - \cos(\theta - \theta_a)}{1 + \sin(\theta - \theta_a)} \right] & \text{if } \theta_a + \pi/2 \leq |\theta| \leq 3\pi/2 - \theta_a \end{cases} \quad (6.2)$$

As observed in Eq. (6.2), the classical 2D-CPC profile only depends on the acceptance angle  $\theta_a$  and on the absorber radius  $r$ . With  $\overline{CC'}$  being the 2D-CPC entrance width, the rod radius is given by Eq. (6.3),

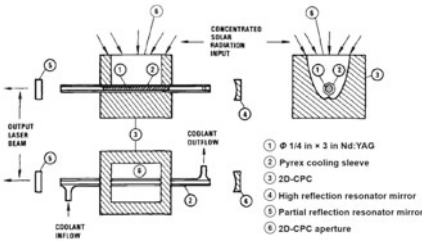
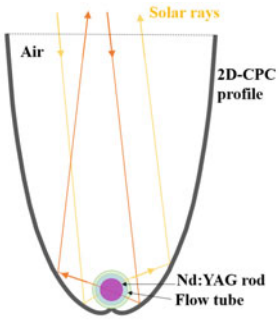
$$2\pi r = \overline{CC'} \sin(\theta_a) \quad (6.3)$$

The 2D-CPC was first implemented in solar-pumped lasers as a secondary concentrator in 1988 by Weksler and Schwartz, to increase the coupling of solar rays from the WIS concentrator into the Nd:YAG rod in a side-pumping configuration [4], as shown in Table 6.7. This has contributed to more than 60 W of solar laser power, the highest to that date. Later, Lando et al. has also utilized this concentrator type at the focus of the ACTA solar concentrator for side-pump Nd:YAG solar laser experiments, achieving 6.7 W/m<sup>2</sup> collection efficiency, which constituted a record in 2003 [7].

### 6.1.4.3 Conical Pump Cavity for End-Side-Pumping Scheme

In the previous works, non-imaging secondary CPCs were used to further concentrate and redistribute the sunlight from primary mirror concentrators along the laser rods in side-pumping configurations [4, 6, 7]. However, the pump radiation passes through the active medium only once in a CPC chamber. Besides, the optical path in side-pumping configuration is less than that in end-pumping configuration, resulting in

**Table 6.7** Milestone solar lasers with secondary two-dimensional compound parabolic concentrators (2D-CPCs)

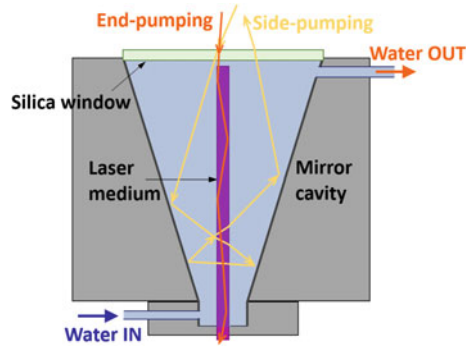
Year	Authors [Ref.]	Milestones
Secondary concentrator (image)		Solar laser system parameters
1988	Weksler and Schwartz [4]	> 60 W Nd:YAG solar laser power
 <p>Primary concentrator, effective collection area: WIS mirror concentrator, ~12.8 m<sup>2</sup></p> <p><b>Secondary concentrator: Dry 2D-CPC</b></p> <p>Active medium: Ø 6.35 mm × 76.2 mm Nd:YAG</p>		
2003	Lando et al. [7]	6.7 W/m <sup>2</sup> Nd:YAG solar laser collection efficiency
 <p>Primary concentrator, effective collection area: WIS ACTA solar concentrator, 6.75 m<sup>2</sup></p> <p><b>Secondary concentrator: Dry 2D-CPC</b></p> <p>Aperture: 98 × 89 mm<sup>2</sup></p> <p>Length: 131 mm</p> <p>Active medium: Ø 10 mm × 130 mm Nd:YAG</p>		

Images adapted from [4] and [7] respectively

lower pumping efficiency. These concerns became even more challenging with the introduction of Fresnel lens as primary concentrator [9], due to the dependence of the focal length on the solar spectrum wavelength. To overcome this issue, in 2007 Yabe et al. adopted a secondary conical mirror to end-side-pump a Cr:Nd:YAG rod at the focus of a 1.3 m<sup>2</sup> Fresnel lens [9], as illustrated in Fig. 6.7.

This type of concentrator provided the confinement of light by multiple reflections inside the pumping cavity, enhancing the absorption efficiency. The solar laser collection efficiency was boosted to 18.7 W/m<sup>2</sup>, representing a 2.8 times enhancement over the previous record of 6.7 W/m<sup>2</sup> by Lando et al. [7]. Since then, the conical cavity has been widely used by solar laser researchers, either as a secondary [9–12] or tertiary concentrator [13, 14, 17–22].

**Fig. 6.7** Schematic design of a secondary conical pump cavity for end-side-pumping, with Fresnel lens primary concentrator (adapted from [10])



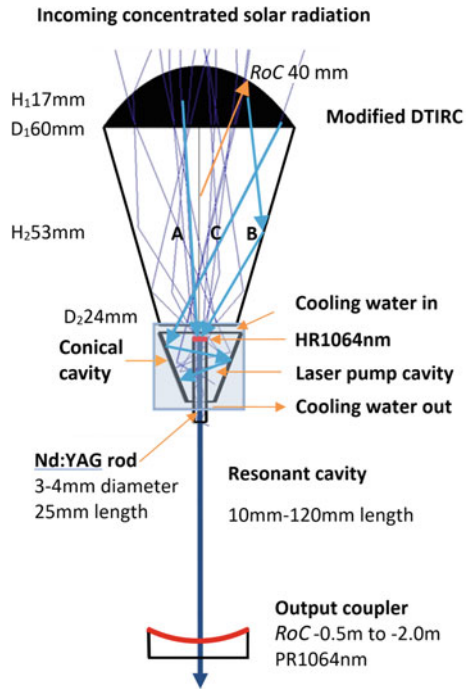
#### 6.1.4.4 Dielectric Totally Internally Reflecting Secondary Concentrator (DTIRC) for End-Side-Pumping Scheme

Dielectric totally internally reflecting concentrator (DTIRC) was originally designed for photovoltaic applications with the goal of reducing the cost of electricity generated through photovoltaic conversion [49]. DTIRCs combine the front surface refraction with total internal reflection from the sidewall to achieve concentrations close to the theoretical limits [50]. Unlike dielectric CPCs, which has a flat front surface, the curved front surface of the DTIRCs works like a lens, concentrating the solar rays before their reflection on the sidewalls. Therefore, the more curved the front surface, the shorter the DTIRC [50].

In 2011, Liang and Almeida employed a modified version of the DTIRC with an aspherical front surface and a conical section to efficiently concentrate the solar radiation from a  $0.636 \text{ m}^2$  Fresnel lens primary concentrator to the upper end-region of the 25 mm length Nd:YAG laser rods with either 3 or 4 mm diameter [13], as illustrated in Fig. 6.8. The previous progress in solar-pumped laser with economical Fresnel lens has revitalized solar laser researches [9]. However, chromatic aberration of the Fresnel lens hinders the coupling of the different solar pump wavelengths into a small laser rod by a conventional lens. The modified DTIRC was therefore designed to overcome this difficulty [13]. For end-pumping, one part of the radiation was directly focused onto the upper end-face of the laser rod through the curved surface of the DTIRC, represented by ray A, while another part was focused indirectly through total internal reflection from the conical section of the DTIRC, represented by ray B. The solar radiation that does not hit the end face of the rod, represented by ray C, was guided into the small conical cavity, ensuring a multi-pass side-pumping to the rod.

As shown in Fig. 6.8, the end face of the DTIRC was in direct contact with cooling water, which ensured an efficient light coupling to the rod. The laser resonator was formed by the high reflection (HR) coating at 1064 nm on the upper end-face of the laser rod and the partial reflection (PR) coating on the concave output mirror. This solar laser system permitted to obtain 12.3 W cw laser power from a

**Fig. 6.8** The Nd:YAG laser head composed of the secondary DTIRC and the tertiary conical concentrator where a 3–4 mm diameter rod is efficiently pumped. RoC, radius of curvature;  $H_1$ , height of the aspherical section of the DTRIC;  $H_2$ , height of the conical section of the DTRIC;  $D_1$ , DTIRC input diameter;  $D_2$ , DTIRC output diameter. HR, high reflection; PR, partial reflection



$\varnothing 4 \text{ mm} \times 25 \text{ mm}$  laser rod, corresponding to a record solar laser collection efficiency of  $19.3 \text{ W/m}^2$  at that time.

### 6.1.5 Tertiary Imaging and Nonimaging Concentrators

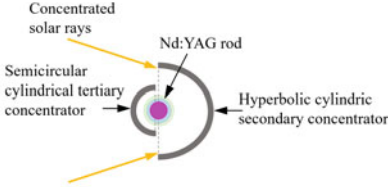
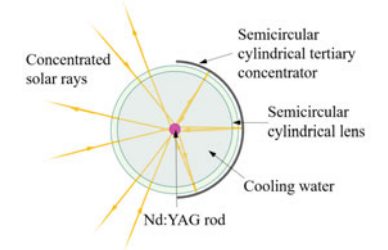
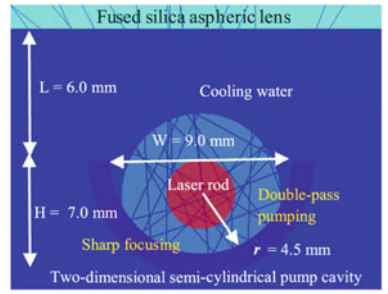
Tertiary concentrators are indispensable for increasing the solar laser pumping efficiency since they can either compress or wrap the solar radiation from the secondary concentrator to the laser medium. The imaging and nonimaging tertiary concentrators that played a key role in the solar laser advances are addressed in this section.

#### 6.1.5.1 Semi-Cylindrical Mirror as an Imaging Tertiary Concentrator

Semi-cylindrical tertiary mirrors have been implemented in some solar laser systems with side-pumping configuration to both redirect and refocus the transmitted solar radiation from imaging secondary concentrators back to the laser rod [2, 3, 15], as summarized in Table 6.8.

This tertiary concentrator was first adopted by Young in 1966 for the first Nd:YAG solar laser emission [2]. To prove the advantage of using the semi-cylindrical mirror,

**Table 6.8** Milestone solar lasers with semi-cylindrical mirror as tertiary concentrators

Year	Authors [Ref.]	Milestones
Secondary concentrator (image)		Solar laser system parameters
1966	Young [2]	First 1 W Nd:YAG solar laser
		Primary concentrator: $\varnothing$ 0.61 m Parabolic mirror Secondary concentrator: Hyperbolic cylindric mirror <b>Tertiary concentrator: Dry semi-cylindrical reflector</b> Active medium: $\varnothing$ 3 mm $\times$ 30 mm Nd:YAG
1984	Arashi et al. [3]	18 W Nd:YAG solar laser power
		Primary Concentrator, effective collection area: TU segmented paraboloidal mirror, $\sim 13.1 \text{ m}^2$ Secondary concentrator: Cylindrical lens <b>Tertiary concentrator: Semi-cylindrical reflector</b> Active medium: $\varnothing$ 4 mm $\times$ 75 mm Nd:YAG
2019	Liang et al. [15]	Side-pumped Nd:YAG solar laser with 5.4% slope efficiency
		Primary Concentrator, effective collection area: FCT NOVA parabolic mirror, $0.9 \text{ m}^2$ Secondary concentrator: Aspherical lens <b>Tertiary concentrator: Water-cooled semi-cylindrical reflector</b> Material: silver-coated aluminum foil Reflectivity: 94% Width W: 9.0 mm Radius of curvature $r$ : 4.5 mm Height H: 7.0 mm Length: 18 mm Active medium: $\varnothing$ 3 mm $\times$ 30 mm Nd:YAG

Images adapted from [2, 3, 15], respectively

Young decided to compare the output performance of the Nd:YAG solar laser system with and without it. This experiment has revealed 1.5 times increase in the laser output power over that obtained with the hyperbolic cylindrical secondary concentrator alone.

In 1984, Arashi et al. placed a semi-cylindrical concentrator just behind the secondary cylindrical lens to refocus the transmitted solar radiation to the side-pumped Nd:YAG laser rod [3]. With this combination, 18 W cw solar laser power was measured, the highest at that time.

In 2019, Liang et al. used a water-cooled semi-cylindrical tertiary concentrator for the most efficient side-pumped solar laser [15]. This pump cavity showed great usefulness in both refocusing and reflecting the pump rays from the secondary aspherical lens towards the Nd:YAG rod. One part of the concentrated solar radiation from the parabolic mirror was directly focused onto the laser rod by the secondary lens, but the pump rays were only partially absorbed. Double-pass pumping was possible by the semi-cylindrical mirror, once it could refocus the transmitted pump rays from the secondary lens back to the laser rod. Besides, a significant part of the pump rays exiting the aspherical lens did not pass directly through the laser rod. Therefore, the tertiary concentrator had also a fundamental role in redirecting those pump rays to the laser rod.

#### **6.1.5.2 Two-Dimensional Compound Parabolic Nonimaging Concentrator (2D-CPC)**

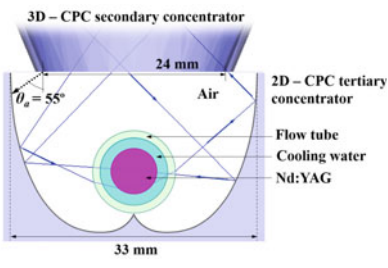
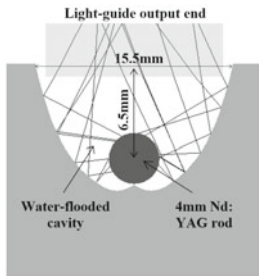
Tertiary concentrators with 2D-CPC shape were also used in conjunction with either secondary 3D-CPCs [6, 7] or rectangular fused silica light-guide homogenizers [23] to side-pump the laser rod, as summarized in Table 6.9.

In 1993 and 2003, Krupkin et al. [6] and Lando et al. [7] combined the 3D-CPC secondary concentrators with 2D-CPC tertiary concentrators for side-pumping of Nd:YAG laser rods. The experimental results from these solar laser systems constituted records in solar laser power [6], collection efficiency [7] and brightness figure of merit [7].

Later, in 2012, Almeida et al. resort a modified version of the classic 2D-CPC as a tertiary concentrator in combination with a secondary fused silica rectangular light guide to improve the absorbed pump distribution along a Nd:YAG laser rod [23].

The classic 2D-CPC design is based on the edge ray principle, which requires the extreme incident rays at the entrance aperture to be tangent to the tubular receiver [44], as demonstrated in Fig. 6.6 (Sect. 6.1.4.2). In a solar laser system, this prevents the most extreme solar rays from being absorbed by the laser medium, impairing the absorption efficiency. The modified 2D-CPC was designed to overcome this drawback, allowing the coupling of the pump rays with high incidence angles coming from the light guide into the laser rod [23]. This design configuration contributed to multimode solar laser beam brightness figure of merit of 0.29 W, which was three times higher than that of the previous solar-pumped Nd:YAG laser by a Fresnel lens [13] and nine times more than that from the previous side-pumped Nd:YAG solar laser with 2D-CPC as tertiary concentrator [7].

**Table 6.9** Milestone solar lasers with two-dimensional compound parabolic concentrators (2D-CPCs) as tertiary concentrators

Year	Authors [Ref.]	Milestones
Secondary concentrator (image)		Solar laser system parameters
2003	Lando et al. [7]	6.7 W/m <sup>2</sup> solar laser collection efficiency 0.032 W multimode solar laser beam brightness
		Primary concentrator, effective collection area: WIS ACTA solar concentrator, 6.75 m <sup>2</sup> Secondary concentrator: 3D-CPC <b>Tertiary concentrator: Dry 2D-CPC</b> Input aperture: 33×24 mm <sup>2</sup> Active medium: Ø 6.0 mm × 72 mm Nd:YAG
2012	Almeida et al. [23]	0.29 W multimode laser beam brightness
		Primary concentrator, effective collection area: PROMES-CNRS parabolic mirror, 2.88 m <sup>2</sup> Secondary concentrator: Rectangular light-guide <b>Tertiary concentrator: Water-flooded 2D-CPC</b> Material: silver-coated aluminum foil Reflectivity: 94% Input aperture: 15.5 × 23 mm <sup>2</sup> Active medium: Ø 4.0 mm × 30 mm Nd:YAG

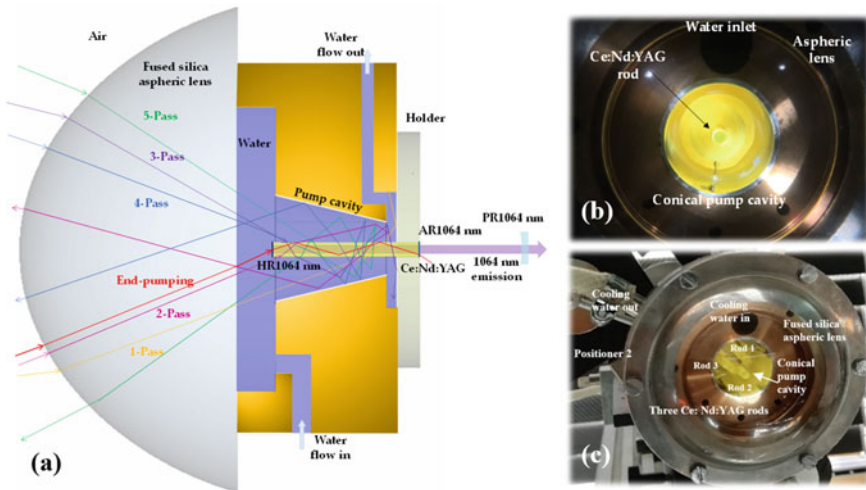
Images adapted from [7] and [23], respectively

### 6.1.5.3 Conical Nonimaging Concentrator for End-Side-Pumping Scheme

Tertiary concentrators with conical shape have been the most widely used in end-side-pumping solar laser systems since the utilization of this type of concentrators in 2007 by Yabe et al. [9]. Conical reflectors of different dimensions have been attached to different secondary concentrators, such as DTRIC [13], aspheric lenses [17–20] and liquid light guide lenses [14, 21, 22], with the common purpose of increasing the absorption efficiency by enabling multi-pass pumping to the laser medium, as shown in Fig. 6.9.

Most of these tertiary concentrators consisted of a silver-coated aluminum foil of 94% reflectivity [13, 17–22] that covered the inner walls of the conical pump cavity. Except the solar laser schemes with a liquid light guide lens as secondary





**Fig. 6.9** **a** Schematic design and **b** front image of the laser head of the most efficient single-rod Ce:Nd:YAG solar laser with primary parabolic mirror concentrator (adapted from [19]). **c** Front image of the laser head of the most efficient solar laser with three Ce:Nd:YAG rods simultaneously pumped (adapted from [20]). Both solar laser prototypes had an aspheric lens and a conical cavity as secondary and tertiary concentrators, respectively

concentrator, which had a dry tertiary conical cavity [14, 21, 22], the remaining prototypes had a water-flooded conical cavity [18–20], as demonstrated in Fig. 6.9.

The use of the conical cavity as a tertiary concentrator contributed to the most important milestone solar lasers in multimode regime:

- The most efficient Nd:YAG solar lasers with parabolic mirror [17] and Fresnel lens [14] as primary concentrators;
- The most efficient Cr:Nd:YAG solar laser [21];
- The most efficient single-rod Ce:Nd:YAG solar laser with primary parabolic mirror concentrator [19], in Fig. 6.9a, b;
- The most efficient simultaneous solar laser emissions with Ce:Nd:YAG as laser media [20], in Fig. 6.9c.

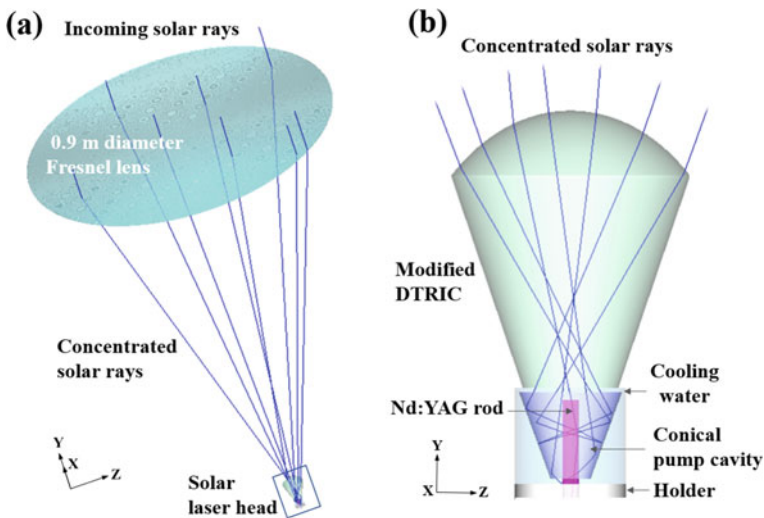
## 6.2 Examples of Numerical Analysis of Milestone Solar-Pumped Lasers

In this section, examples of the modelling and numerical analysis of some milestone solar-pumped lasers are given. The design parameters of the solar laser prototypes here presented were first optimized in Zemax<sup>®</sup> ray-tracing software in non-sequential mode. LASCAD<sup>™</sup> laser cavity analysis software was then used to find out the optimum laser resonator parameters.

### 6.2.1 Zemax<sup>®</sup> and LASCAD<sup>™</sup> Numerical Analysis of 12.3 W Solar Laser with DTIRC Secondary and Conical Tertiary Concentrators

The layout from Zemax<sup>®</sup> of the 12.3 W solar laser [13] is represented in Fig. 6.10. It was composed of the 0.9 m diameter Fresnel lens primary concentrator, the DTIRC secondary concentrator and the conical tertiary mirror, within which the 4 mm diameter, 25 mm length, 1.0 at.% Nd:YAG laser rod was end-side-pumped. This design configuration contributed to the record in solar laser collection efficiency of  $19.3 \text{ W/m}^2$  with Nd:YAG laser medium in 2011 [13].

For modeling the solar laser system, its components are defined by the non-sequential objects of Zemax<sup>®</sup> in the Non-Sequential Component Editor window, as



**Fig. 6.10** Shaded model layout of the 12.3 W solar laser components [13]: **a** Solar laser system; **b** Laser head with the fused silica modified DTIRC and the conical tertiary mirror

Non-Sequential Component Editor			
Edit Solves Tools View Help			
Object Type	Comment		Material
1 Source Ellipse	Solar source		-
2 Fresnel 1	Primary concentrator		PMMA
3 Annular Aspheric Lens	DTIRC (Aspheric lens)		SILICA
4 Cylinder Volume	DTIRC (Conical section)		SILICA
5 Cylinder Volume	Cooling water		WATER
6 Cylinder Pipe	Conical pump cavity		MIRROR
7 Cylinder Volume	Rod holder		MIRROR
8 Detector Volume	Transversal Nd:YAG detector		WATER
9 Detector Volume	Longitudinal Nd:YAG detector		WATER
10 Cylinder Volume	Nd:YAG rod		NDYAG_1.0AT%

**Fig. 6.11** List of Zemax® objects in the non-sequential component editor to simulate the components of the 12.3 W solar laser [13]

explained in Sect. 2.1.1.1 of Chap. 2. The list of Zemax® non-sequential objects utilized to design the 12.3 W solar laser system, as well as the respective materials, are given in Fig. 6.11.

For the light source, 22 peak absorption wavelengths of the Nd:YAG material were added in the source wavelength data: 527, 531, 569, 579, 586, 592, 732, 736, 743, 746, 753, 758, 790, 793, 803, 805, 808, 811, 815, 820, 865, and 880 nm. The weight of each wavelength was defined based on its spectral irradiance value in the standard direct solar spectrum for one-and-a-half air mass (AM1.5 D) [51]. The absorption coefficients of each of those wavelengths [52] were defined in the glass catalog data for the 1.0 at.% Nd:YAG (see Sects. 2.1.1.2 and 2.1.1.4 of Chap. 2 for more details). The absorption spectra and wavelength-dependent refractive indices of PMMA, fused silica and water [19] were also included in the glass catalog data to account for absorption losses in those media. For the conical tertiary concentrator, 94% reflectivity was assumed [13], using the coating I.06 in the section Coat/Scatter of the object properties (see Sect. 2.1.1.3 of Chap. 2 for more details).

The X, Y, Z positions and directions (Tilt About X, Y and Z) of the 12.3 W solar laser components in Zemax® space are indicated in Fig. 6.12. The optimal parameters of the 12.3 W solar laser [13] components defined in Zemax® are indicated in Table 6.10.

For the ray-tracing analysis of the absorbed pump power and light distribution within the active medium, detector volumes divided into several voxels were used. The number of analysis rays in the source and the number of voxels in the detectors were adjusted in order to attain accurate results and good image resolution. To estimate the absorbed pump power by the laser rod, the radiation absorbed in each voxel was summed up.

Figure 6.13 shows the absorbed pump flux distributions along seven transversal cross sections and one longitudinal central cross section of the 4 mm diameter, 25 mm length, 1.0 at.% Nd:YAG laser rod. Red color means near maximum pump

Non-Sequential Component Editor

Object Type	X Position	Y Position	Z Position	Tilt About X	Tilt About Y	Tilt About Z
1 Source Ellipse	852.100	1988.000	7.000	90.000	0.000	0.000
2 Fresnel l	852.100	1987.000	7.000	-90.000	180.000	-90.000
3 Annular Aspheric Lens	852.100	793.690	7.000	-90.000	0.000	0.000
4 Cylinder Volume	852.100	740.700	7.000	-90.000	0.000	0.000
5 Cylinder Volume	852.100	716.800	7.000	-90.000	0.000	0.000
6 Cylinder Pipe	852.100	718.100	7.000	-90.000	0.000	0.000
7 Cylinder Volume	852.100	713.050	7.000	-90.000	0.000	0.000
8 Detector Volume	852.100	725.500	7.000	90.000	0.000	0.000
9 Detector Volume	852.100	725.500	7.000	180.000	90.000	0.000
10 Cylinder Volume	852.100	713.000	7.000	-90.000	0.000	0.000

**Fig. 6.12** Example of the position and rotation of the 12.3 W solar laser [13] components in Zemax® non-sequential component editor

absorption, whereas blue means little or no absorption. The 4 mm diameter, 25 mm length 1.0 at.% Nd:YAG rod absorbed a maximum power of 48.6 W. Due to the rotational symmetry of the end-side-pumping configuration, a symmetric absorbed pump profile was attained. In the central region of the laser rod, maximum absorbed pump intensity of  $0.436 \text{ W/mm}^3$  was detected.

The absorbed pump flux data from the Zemax® analysis was then processed by LASCAD™ to quantify the thermal effects applied in the active medium, previously defined in LASCAD™ (see Sects. 2.2.3 and 2.2.4 of Chap. 2 for more details). A fluorescence lifetime of  $230 \mu\text{s}$  [42] and the mean absorbed and intensity-weighted solar pump wavelength of 660 nm [4] were considered. These values were used for the LASCAD™ numerical analysis of all the solar laser schemes [13, 17, 20, 23]. The reported values of the Nd:YAG stimulated emission cross-section range from 2.7 to  $8.8 \times 10^{-19} \text{ cm}^2$  [53]. Therefore, the value of the stimulated emission cross-section used in LASCAD™ depended on the values given by the laser rod manufacturers. In the present case, a stimulated emission cross-section of  $2.8 \times 10^{-19} \text{ cm}^2$  was assumed [13].

Based on the information from the Finite Element Analysis (FEA) of LASCAD™, the optimal laser resonator beam parameters, represented in Fig. 6.14, were found.

The high reflection (HR 1064 nm) coating on the end face of the laser rod and the partial reflection (PR 1064 nm) coating on the output mirror, together with the Nd:YAG laser rod, formed the laser resonator.  $L_{\text{ROD}}$  represents the rod length and  $L$  represents the separation length between the antireflection (AR 1064 nm) coating on the end face of the rod and the PR 1064 nm output mirror. In the experiments, maximum laser power of 12.3 W was extracted from a PR mirror with 98% reflectivity (R) and  $-0.5 \text{ m}$  radius of curvature (RoC).

For accurate calculation of the laser power in LASCAD™, a simulation of the laser beam profile, based on the beam propagation method (BPM), was performed to find the correct laser beam width at the output mirror. The following procedure (also explained in Sect. 2.3.2 of Chap. 2) was adopted:

1. Accounting for apertures in the laser resonator (Fig. 6.15).
2. Starting BPM analysis (see Sect. 2.2.5 of Chap. 2 for more details).

**Table 6.10** 12.3 W solar laser [13] components defined in Zemax® non-sequential component editor

Solar source							
Parameters Object Type	Analysis Rays	Power (W)	X / Y Half Width (mm)		Gauss G <sub>x</sub> / G <sub>y</sub>		
<b>Source Ellipse</b>	20000000	90.545 <sup>1</sup>	450 / 450		40000 / 40000 <sup>2</sup>		
Primary concentrator							
Parameters Object Type	Radial Height (mm)	X Half-Width (mm)	+Depth/-Freq	Pitch (deg)	Thickness (mm)	Radius (mm)	Conic
<b>Fresnel l<sup>3</sup></b>	450	0	0.3	12	3	640	-0.7
DTIRC (Aspherical lens section)							
Parameters Object Type	Min / Max Front Aper (mm)	Min / Max Back Apert (mm)	Thick Aper (mm)	Rear Radius (mm)	Rear Conic	Thickness (mm)	Rear r <sup>2</sup>
<b>Annular Aspheric Surface</b>	0 / 30	0 / 30	0	-40	0	17	-0.003
DTIRC (Conical section)							
Parameters Object Type	Front R (mm)		Z Length (mm)		Back R (mm)		
<b>Cylinder Volume</b>	12		53		30		
Cooling water							
Parameters Object Type	Front R (mm)		Z Length (mm)		Back R (mm)		
<b>Cylinder Volume</b>	14		24		14		
Conical pump cavity							
Parameters Object Type	Front R (mm)		Z Length (mm)		Back R (mm)		
<b>Cylinder Pipe</b>	5		22		12		
Rod holder							
Parameters Object Type	Front R (mm)		Z Length (mm)		Back R (mm)		
<b>Cylinder Volume</b>	14		3.8		14		
Transversal detector							
Parameters Object Type	X / Y / Z Half Width (mm)			# X / # Y / # Z Pixels			
<b>Detector Volume</b>	2 / 2 / 12.5			80 / 80 / 25			
Longitudinal detector							
Parameters Object Type	X / Y / Z Half Width (mm)			# X / # Y / # Z Pixels			
<b>Detector Volume</b>	2 / 12.5 / 2			40 / 250 / 5			
1.0 at.% Nd:YAG rod							
Parameters Object Type	Front R (mm)		Z Length (mm)		Back R (mm)		
<b>Cylinder Volume</b>	2		25		2		

<sup>1</sup> The source power was calculated by using Eq. (2.4) from Chap. 2:  $P_{source, Nd:YAG} = A_{ef} \times I_s \times \eta_{overlap, Nd^{3+}}$ .

$A_{ef} = 0.636 \text{ m}^2$  is the effective collection area of primary Fresnel lens concentrator with 0.9 m in diameter.  $I_s$  is the solar irradiance, whose reported value was 890 W/m<sup>2</sup> [13].  $\eta_{overlap, Nd^{3+}}$  is the spectral overlap of the Nd<sup>3+</sup> absorption spectrum with solar emission spectrum, which is 16% (See Sect. 4.3.2 of Chap. 4).

<sup>2</sup>  $G_x$  and  $G_y$  parameters define the Gaussian distribution of the solar rays in X and Y axes.  $G_x = G_y = 40,000$  were defined to account for the apparent half angle of 0.27° subtended by the Sun on the Earth surface.

<sup>3</sup> The parameters of a Fresnel lens are described in Sect. 5.2 of Chap. 5.

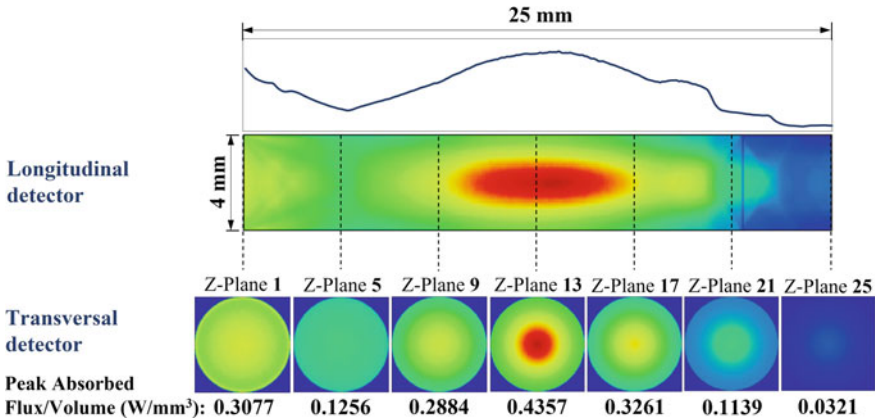


Fig. 6.13 Absorbed pump flux distributions along the longitudinal central cross-section and seven transversal cross sections of the 4.0 mm diameter, 25 mm length, 1.0 at.% Nd:YAG rod of the 12.3 W solar laser [13], obtained through Zemax<sup>®</sup> numerical analysis

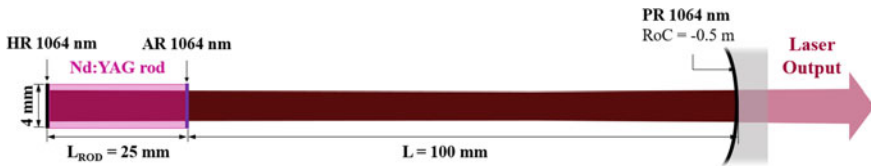
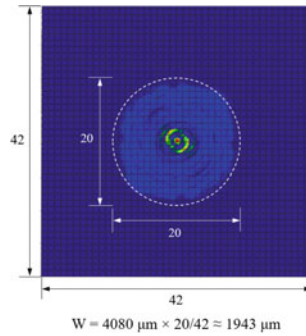


Fig. 6.14 Schematic design of the 12.3 W solar laser resonator [13]. The image is not at scale

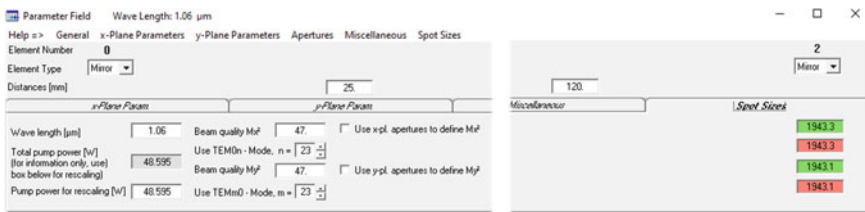


Fig. 6.15 Accounting for apertures in the 12.3 W solar laser resonator [13] in LASCAD™ *Parameter Field*

3. Finding the beam waist,  $W$ , of the laser beam profile. It is calculated by multiplying the half width of the BPM computational window ( $4080 \mu\text{m}$ ) by the quotient between the number of squares of the grid representing the maximum oscillating laser modes in X, Y directions ( $\sim 20$  squares) and the total number of squares in the grid (42 squares), illustrated in Fig. 6.16.
4. Modifying the  $M_x^2$ ,  $M_y^2$  factors in the *Parameter Field* window until the spot sizes are coincident with the beam waist from BPM analysis, as illustrated in Fig. 6.17.



**Fig. 6.16** Top-view of the 12.3 W solar laser beam profile from BPM analysis of LASCAD™

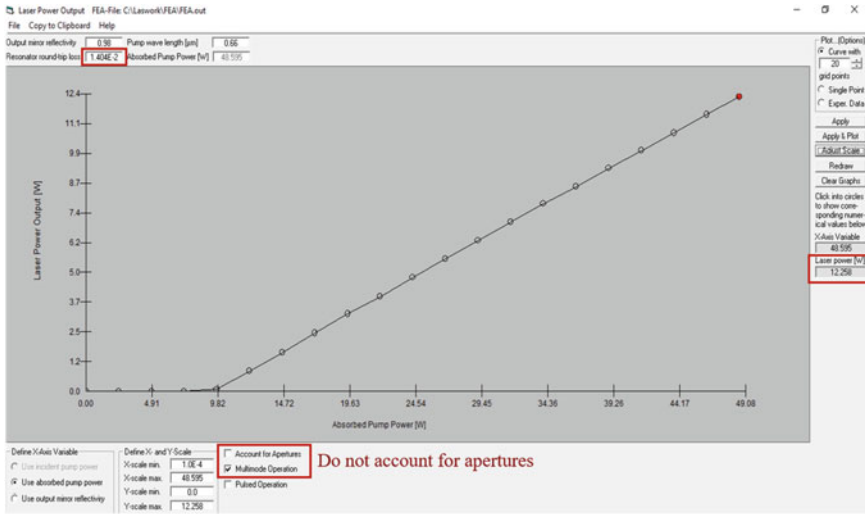


**Fig. 6.17** Correction of the beam waist in LASCAD™ *Parameter Field* by changing the  $M_x^2$ ,  $M_y^2$  factors

- Calculating multimode laser power in the *Laser Output Power* window, with account for apertures unchecked, as indicated in Fig. 6.18.

For accurate calculation of the laser power, the total roundtrip losses (given by Eq. (2.7) in Chap. 2) must be defined in this window. By considering a typical absorption and scattering loss  $\alpha$  of  $0.002 \text{ cm}^{-1}$ , a two-way loss of 1% was found for the 4.0 mm diameter, 1.0 at.% Nd:YAG rod with 2.5 cm length. Assuming 0.4% of imperfect HR and AR coatings, the total round-trip loss increased to 1.4%. The diffraction losses depend on rod diameter, resonator length and radius of curvature (RoC) of the resonator mirrors. For the present solar laser resonator, 0.04% of diffraction losses was calculated by LASCAD™ BPM analysis. A total round-trip loss of 1.404% was hence defined in the *Laser Output Power* window (Fig. 6.18).

Based on this procedure, 12.26 W was numerically obtained from an output mirror with  $R = 98\%$  and  $\text{RoC} = -0.5 \text{ m}$ , matching well with the experimental solar laser power value with similar PR mirror characteristics [13].



**Fig. 6.18** Numerically calculated laser output power in LASCAD™ as a function of the absorbed solar power, for the output mirror reflectivity ( $R$ ) of 98%

### 6.2.2 Zemax® and LASCAD™ Numerical Analysis of 28 W Solar Laser with a Fused Silica Light Guide Homogenizer and a 2D-CPC Pump Cavity

The layout from Zemax® of the 28 W solar laser [23] is represented in Fig. 6.19. The fused silica light guide of 14 mm × 22 mm rectangular cross-section was used to both transmit and homogenize, through total internal reflection, the concentrated solar radiation from the focal zone of the 2.0 m diameter parabolic mirror to the entrance aperture of a modified 2D-CPC water-flooded pump cavity, within which the 4 mm diameter, 30 mm length, 1.1 at.% Nd:YAG laser rod was side-pumped. This design configuration contributed to record solar laser brightness figure of merit of 0.29 W in 2012 [23].

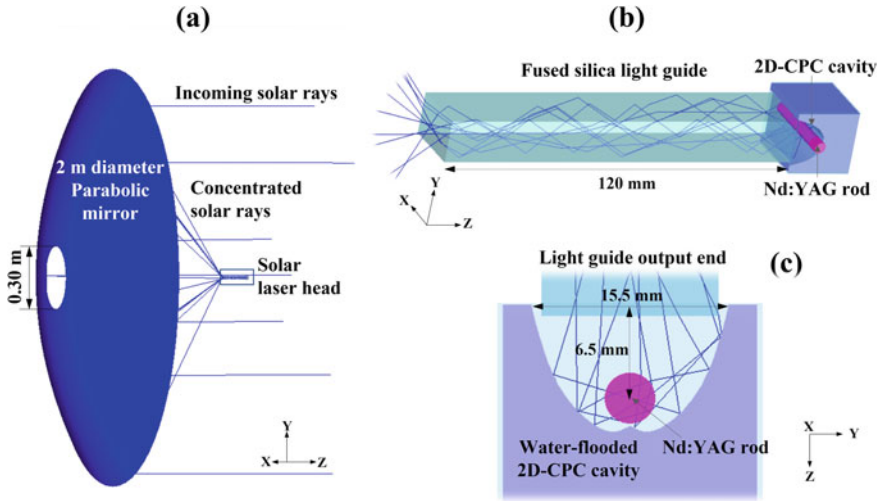
The list of Zemax® non-sequential objects utilized to design the 28 W solar laser components, as well as the respective materials, are given in Fig. 6.20.

The X, Y, Z positions and directions (Tilt about X, Y and Z) of the 28 W solar laser components in Zemax® space are indicated in Fig. 6.21.

The optimal parameters of the 28 W solar laser [23] components defined in Zemax® are indicated in Table 6.11.

All the solar laser components were parameterized using objects existent in the Zemax® list, except for the 2D-CPC pump cavity, which was designed in AUTOCAD and imported to Zemax® (see Sect. 2.1.3.2 of Chap. 2 for more details). The solar wavelength data and the media materials were defined in the same way as in the previous example in Sect. 6.2.1. For the primary concentrator, 64% reflectivity was assumed, which accounted for the absorption losses in both the heliostat and parabolic





**Fig. 6.19** Shaded model layout of the 28 W solar laser components [23]: **a** Solar laser system; **b** Laser head with the fused silica light guide homogenizer and the 2D-CPC pump cavity; **c** Detailed view of the modified 2D-CPC pump cavity

Non-Sequential Component Editor

Object Type	Comment	Material
1 Source Ellipse	Solar source	-
2 Aspheric Surface	Primary concentrator	MIRROR
3 Rectangular Volume	Cooling water	WATER
4 Rectangular Volume	Rectangular light guide	SILICA
5 Detector Volume	Transversal Nd:YAG detector	WATER
6 Detector Volume	Longitudinal Nd:YAG detector	WATER
7 Cylinder Volume	Nd:YAG rod	NDYAG_1.1AT%
8 CAD Part: STL	Modified 2D-CPC.STL	MIRROR

**Fig. 6.20** List of Zemax® objects in the non-sequential component editor to simulate the components of the 28 W solar laser [23]

Non-Sequential Component Editor

Object Type	X Position	Y Position	Z Position	Tilt About X	Tilt About Y	Tilt About Z
1 Source Ellipse	0.000	0.000	1310.00	180.000	0.000	0.000
2 Aspheric Surface	0.000	0.000	0.000	0.000	0.000	0.000
3 Rectangular Volume	-11.500	0.000	979.000	90.000	90.000	0.000
4 Rectangular Volume	0.000	0.000	849.500	0.000	0.000	90.000
5 Detector Volume	0.000	0.000	976.000	-90.000	90.000	0.000
6 Detector Volume	0.000	0.000	976.000	0.000	0.000	90.000
7 Cylinder Volume	-15.000	0.000	976.000	0.000	90.000	0.000
8 CAD Part: STL	13.500	12.050	991.500	180.000	0.000	90.000

**Fig. 6.21** Example of the position and rotation of the 28 W solar laser [23] components in Zemax® non-sequential component editor

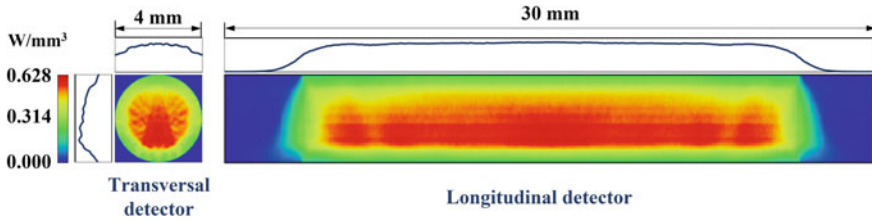
**Table 6.11** 28 W solar laser [23] components defined in Zemax® non-sequential component editor

Solar source				
Parameters Object Type	Power (W)	X / Y Half Width (mm)	Gauss Gx / Gy	Minimum X / Y Half Width (mm)
<b>Source Ellipse</b>	456.2 <sup>1</sup>	1000 / 1000	40000 / 40000	150 / 150 <sup>2</sup>
Primary concentrator				
Parameters Object Type	Radius (mm)	Conic	Max / Min Aper (mm)	
<b>Aspheric Surface</b> <sup>3</sup>	1700	-1	1000 / 150	
Cooling water				
Parameters Object Type	X1 / Y1 Half Width (mm)	Z Length (mm)	X2 / Y2 Half Width (mm)	
<b>Rectangular Volume</b>	10.5 / 10.5	23	10.5 / 10.5	
Rectangular light guide				
Parameters Object Type	X1 / Y1 Half Width (mm)	Z Length (mm)	X2 / Y2 Half Width (mm)	
<b>Rectangular Volume</b>	7 / 11	120	7 / 11	
Transversal detector				
Parameters Object Type	X / Y / Z Half Width (mm)		# X / # Y / # Z Pixels	
<b>Detector Volume</b>	2 / 2 / 15		80 / 80 / 30	
Longitudinal detector				
Parameters Object Type	X / Y / Z Half Width (mm)		# X / # Y / # Z Pixels	
<b>Detector Volume</b>	2 / 15 / 2		40 / 300 / 5	
1.1 at.% Nd:YAG rod				
Parameters Object Type	Front R (mm)	Z Length (mm)	Back R (mm)	
<b>Cylinder Volume</b>	2	30	2	
Modified 2D-CPC				
Parameters Object Type	Scale		Is Volume?	
<b>CAD Part: STL</b>	1		1	

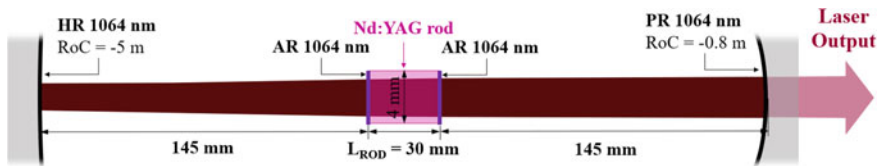
<sup>1</sup> For the 28 W solar laser, an effective collection area of 2.88 m<sup>2</sup> and maximum direct solar irradiance of 990 W/m<sup>2</sup> were measured [23]. Therefore,  $P_{source, Nd:YAG} = 2.88 \text{ m}^2 \times 990 \text{ W.m}^{-2} \times 0.16 = 456.2 \text{ W}$  was calculated.

<sup>2</sup> Minimum X/Y Half Width of 150 mm was defined in the source, since the solar rays from this region are not collected by the primary parabolic mirror, which has a central hole of 300 mm in diameter (Fig. 6.19).

<sup>3</sup> The parameters of a parabolic mirror are described in Sect. 5.1 of Chap. 5.



**Fig. 6.22** Absorbed pump flux distributions along the central transversal and longitudinal cross-sections of the 4.0 mm diameter, 30 mm length, 1.1 at.% Nd:YAG rod of the 28 W solar laser [23], obtained through Zemax<sup>®</sup> numerical analysis



**Fig. 6.23** Schematic design of the 28 W solar laser resonator [23]. The image is not at scale

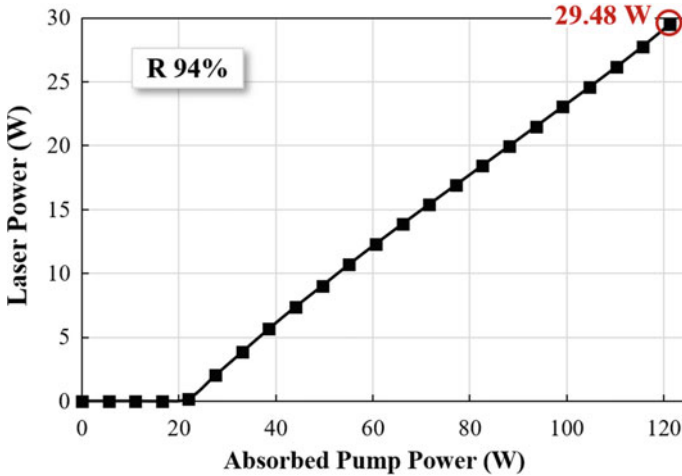
mirrors [23]. Therefore, the coating I.36 was defined in the section Coat/Scatter of the object properties. For the 2D-CPC, 94% reflectivity (I.06) was considered [23].

The absorbed pump flux distributions along one central transversal cross section and one central longitudinal cross section of the 4 mm diameter, 30 mm length, 1.1 at.% Nd:YAG laser rod is shown in Fig. 6.22. The rectangular fused silica light guide behaved like a beam homogenizer by transforming the near-Gaussian profile of the concentrated light spot from the parabolic mirror, incident on its input face, into a uniform rectangular light distribution at its output end [23], enabling a homogeneous absorbed pump light distribution along the Nd:YAG laser rod, as demonstrated in Fig. 6.22. This helps to reduce the thermal induced effects in the laser rod and meliorate the laser beam quality. Therefore, the output laser beam brightness can be higher compared to solar lasers with no light homogenizer [7, 13].

The modified 2D-CPC also played a crucial role in improving the absorbed pump distribution by coupling efficiently the pump rays into the center of the laser rod, as shown by the transversal cross-section (Fig. 6.22).

A symmetric concave-concave laser resonator of 320 mm length was adopted in this case, as illustrated in Fig. 6.23. The HR coated mirror with  $\text{RoC} = -5$  m, the Nd:YAG laser rod and the PR mirror formed the laser resonator. The PR mirror with  $R = 94\%$  and  $\text{RoC} = -0.8$  m led to the maximum measured laser output power of 27.7 W [23].

In the present case, a stimulated emission cross-section of  $2.8 \times 10^{-19} \text{ cm}^2$  was assumed for LASCAD<sup>™</sup> analysis [23]. Based on the procedure described in 6.2.1, multimode laser output power of 29.48 W was numerically extracted from the PR mirror with  $R = 94\%$  and  $\text{RoC} = -0.8$  m at maximum absorbed pump power of 121.2 W, as shown in Fig. 6.24, which agrees reasonably well with the experimental value [23].



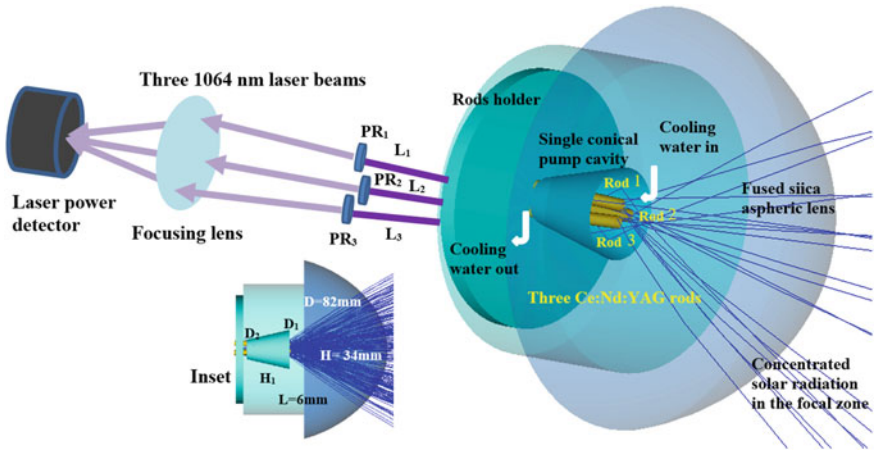
**Fig. 6.24** Numerically calculated laser output power from the 4 mm diameter, 30 mm length, 1.1 at.% Nd:YAG rod in LASCAD™ as a function of the absorbed solar power, for the output mirror reflectivity (R) of 94%

### 6.2.3 *Zemax® and LASCAD™ Numerical Analysis of Simultaneous Solar Laser Emissions from Three Ce:Nd:YAG Laser Rods Within a Single Pump Cavity*

The design of the 16.5 W solar laser [20], composed of the 0.8 m diameter parabolic mirror as primary concentrator, the secondary aspheric lens and the conical tertiary mirror, within which the three 2.5 mm diameter, 25 mm length, 0.1 at.% Ce: 1.1 at.% Nd:YAG laser rods were end-side-pumped, is represented in Fig. 6.25. This design configuration contributed to the current records in solar-to-laser conversion, collection and slope efficiencies of 4.64%, 41.25 W/m<sup>2</sup> and 7.64%, respectively [20].

The list of Zemax® non-sequential objects utilized to design the 16.5 W three-rod Ce:Nd:YAG solar laser system, as well as the respective materials, are given in Fig. 6.26.

In this case, two sources were defined. Source 1 represents the relevant solar emission wavelengths that overlaps with the Nd<sup>3+</sup> ion absorption spectrum, as well as those correspondent to the Ce<sup>3+</sup> non-radiative transfer to Nd<sup>3+</sup> by quantum cutting down conversion. Source 2 is related to the solar wavelengths corresponding to the radiative transfer from Ce<sup>3+</sup> to Nd<sup>3+</sup> (see Sect. 4.5 of Chap. 4 for more details). For such, the wavelength data was defined in two spectrum files, one for each source. The spectrum file for source 1 is similar to the wavelength data of the previous examples, i.e., with 22 peak absorption wavelengths of Nd<sup>3+</sup>, whose weight is decided by the solar spectral irradiance value. For source 2, six wavelengths were defined in the spectrum file, corresponding to the most relevant Nd<sup>3+</sup> peak absorption wavelengths that matches with the Ce<sup>3+</sup> fluorescence spectrum: 527, 531, 569, 579, 586, and



**Fig. 6.25** Design of the three-rod Ce: Nd:YAG laser head, composed of the fused silica aspheric lens, the conical pump cavity and the Ce:Nd:YAG rods, actively cooled by water [20]

Non-Sequential Component Editor

Edit Solves Tools View Help

Object Type	Comment	Material
1 Source Ellipse	Nd absorption spectrum	-
2 Source Ellipse	Ce fluorescence spectrum	-
3 Aspheric Surface	Primary concentrator	MIRROR
4 Annular Aspheric Lens	Aspheric lens	SILICA
5 Cylinder Volume	Cooling water	WATER
6 Cylinder Volume	3-Rod holder	MIRROR
7 Detector Volume	Transversal rod 1 detector	WATER
8 Cylinder Volume	Rod 1	NDYAG_1.1AT%
9 Detector Volume	Transversal rod 2 detector	WATER
10 Cylinder Volume	Rod 2	NDYAG_1.1AT%
11 Detector Volume	Transversal rod 3 detector	WATER
12 Cylinder Volume	Rod 3	NDYAG_1.1AT%
13 Cylinder Pipe	Conical pump cavity	MIRROR

**Fig. 6.26** List of Zemax® objects in the Non-Sequential Component Editor to simulate the components of the most efficient solar laser from three Ce:Nd:YAG rods [20]

592 nm [19, 20]. In this case, the weight of each wavelength was defined based on its spectral irradiance in the  $Ce^{3+}$  fluorescence spectrum [54]. It is worth noting that the  $Nd^{3+}$  material programmed in the glass catalog data in Zemax® software can also be used to represent the Ce:Nd:YAG material. This is possible thanks to the energy transfer mechanism from  $Ce^{3+}$  to  $Nd^{3+}$  ions in Ce:Nd:YAG medium.

For the primary concentrator, 75% reflectivity was assumed, which accounted for the absorption losses in both the heliostat and parabolic mirrors [20]. Therefore, the

Object Type	X Position	Y Position	Z Position	Tilt About X	Tilt About Y	Tilt About Z
1 Source Ellipse	852.100	855.900	1000.000	180.000	0.000	90.000
2 Source Ellipse	852.100	855.900	1000.000	180.000	0.000	90.000
3 Aspheric Surface	852.100	855.900	-648.000	0.000	0.000	0.000
4 Annular Aspheric Lens	852.100	855.900	0.000	180.000	0.000	0.000
5 Cylinder Volume	852.100	855.900	0.000	0.000	0.000	0.000
6 Cylinder Volume	852.100	855.900	27.000	0.000	0.000	0.000
7 Detector Volume	852.100	853.481	18.488	2.400	0.000	45.000
8 Cylinder Volume	852.100	854.005	6.000	2.400	0.000	0.000
9 Detector Volume	854.207	857.087	18.488	-1.200	2.078	75.000
10 Cylinder Volume	853.754	856.825	6.000	-1.200	2.078	0.000
11 Detector Volume	849.994	857.087	18.488	-1.200	-2.078	15.000
12 Cylinder Volume	850.446	856.825	6.000	-1.200	-2.078	0.000
13 Cylinder Pipe	852.100	855.900	6.500	0.000	0.000	0.000

**Fig. 6.27** Example of the position and rotation of the most efficient solar laser emissions from three Ce:Nd:YAG rods [20] in Zemax® Non-Sequential Component Editor

coating I.25 was defined in the section Coat/Scatter of the object properties. For the conical pump cavity, 94% reflectivity (I.06) was considered [20].

The X, Y, Z positions and directions (Tilt about X, Y and Z) of the simultaneous 16.5 W solar laser system in Zemax® space are indicated in Fig. 6.27. The optimal parameters of the simultaneous 16.5 W solar laser [20] components defined in Zemax® are indicated in Table 6.12.

The absorbed pump flux distributions along five transversal cross-sections of the three Ce:Nd:YAG rods are given in Fig. 6.28. Non-uniform distributions along the end-side-pumped laser rods were numerically calculated with a peak absorbed pump flux of 0.68 W/mm<sup>3</sup>. Nevertheless, these were the distributions that ensured the maximum absorbed solar power by the three rods.

In the present case, a stimulated emission cross-section of  $2.8 \times 10^{-19}$  cm<sup>2</sup> was assumed for LASCAD™ analysis [20]. The laser resonator configuration for maximum multimode solar laser extraction from one of the three Ce:Nd:YAG laser rods is illustrated in Fig. 6.29, which is similar for all the three laser rods. PR mirrors with 97.5% reflectivity and RoC = -0.5 m were adopted. Each one was optically aligned with its respective laser rod 15 mm away from the AR1064 nm output face.

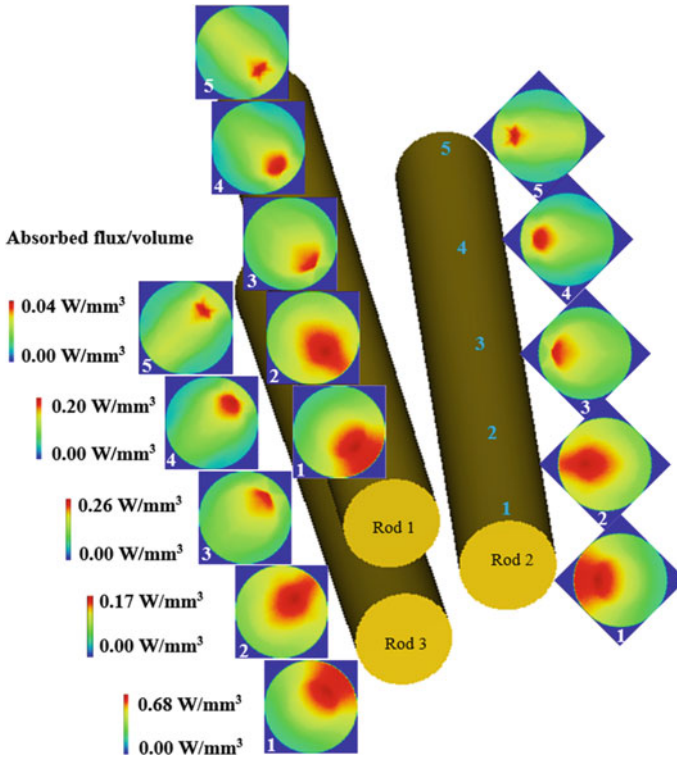
With this laser resonator configuration, maximum multimode laser power of 5.64 W was numerically calculated for each one of the Ce:Nd:YAG rods, as shown in Fig. 6.30, corresponding to 16.92 W (3 × 5.64 W) total multimode solar power, which is close to the experimental value of 16.5 W.

**Table 6.12** Components of the most efficient solar laser emissions from three Ce:Nd:YAG rods [20] defined in non-sequential component editor

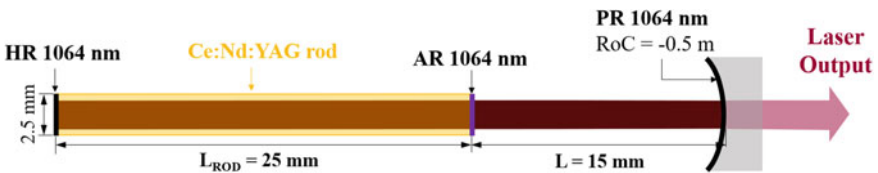
Solar source (Nd <sup>3+</sup> absorption spectrum)							
Parameters Object Type	Power (W)	X / Y Half Width (mm)		Gauss Gx / Gy			
Source Ellipse	95.15 <sup>1</sup>	400 / 400		40000 / 40000			
Solar source (Ce <sup>3+</sup> fluorescence spectrum)							
Parameters Object Type	Power (W)	X / Y Half Width (mm)		Gauss Gx / Gy			
Source Ellipse	16.35 <sup>2</sup>	400 / 400		40000 / 40000			
Primary concentrator							
Parameters Object Type	Radius (mm)	Conic		Max / Min Aper (mm)			
Aspheric Surface	1320	-1		410 / 0			
Aspherical lens							
Parameters Object Type	Min / Max Front Aper (mm)	Min / Max Back Aper (mm)	Thick Aper (mm)	Rear Radius (mm)	Rear Conic	Thickness (mm)	Rear r <sup>2</sup>
Annular Aspheric Surface	0 / 41	0 / 41	0	-43	0	37	-0.004
Cooling water							
Parameters Object Type	Front R (mm)	Z Length (mm)		Back R (mm)			
Cylinder Volume	35	27		35			
3-Rod holder							
Parameters Object Type	Front R (mm)	Z Length (mm)		Back R (mm)			
Cylinder Volume	20	3.5		20			
Transversal detectors of Rods 1, 2 and 3							
Parameters Object Type	X / Y / Z Half Width (mm)			# X / # Y / # Z Pixels			
Detector Volume	1.25 / 1.25 / 12.5			50 / 50 / 25			
Ce:Nd:YAG laser rods							
Parameters Object Type	Front R (mm)	Z Length (mm)		Back R (mm)			
Cylinder Volume	1.25	25		1.25			
Conical pump cavity							
Parameters Object Type	Front R (mm)	Z Length (mm)		Back R (mm)			
Cylinder Pipe	9	19		4.5			

<sup>1</sup> The source1 power was calculated by using Eq. (2.5) from Chap. 2:  $P_{source1, Ce:Nd:YAG} = A_{ef} \times I_s \times (\eta_{overlap, Nd^{3+}} + \eta_{overlap, Ce^{3+}} \times \eta_{NR: Ce^{3+} \rightarrow Nd^{3+}})$ , where  $\eta_{overlap, Ce^{3+}} = 15.3\%$  is the spectral overlap of the Ce<sup>3+</sup> absorption spectrum with the solar emission spectrum and  $\eta_{NR: Ce^{3+} \rightarrow Nd^{3+}} = 70\%$  is the percentage of absorbed energy by Ce<sup>3+</sup> ions that could be transferred to Nd<sup>3+</sup> non-radiatively [19, 20]. Since  $A_{ef} = 0.4 \text{ m}^2$  and  $I_s = 890 \text{ W/m}^2$  were accounted [20], then  $P_{source1, Ce:Nd:YAG} = 95.15 \text{ W}$  was calculated.

<sup>2</sup> The source2 power was calculated by using Eq. (2.6) from Chap. 2:  $P_{source2, Ce:Nd:YAG} = A_{ef} \times I_s \times \eta_{overlap, Ce^{3+}} \times \eta_{R: Ce^{3+} \rightarrow Nd^{3+}}$ , where  $\eta_{R: Ce^{3+} \rightarrow Nd^{3+}} = 30\%$  is the percentage of absorbed energy by Ce<sup>3+</sup> ions that could be transferred to Nd<sup>3+</sup> radiatively [19, 20].  $P_{source1, Ce:Nd:YAG} = 16.35 \text{ W}$  was hence calculated.

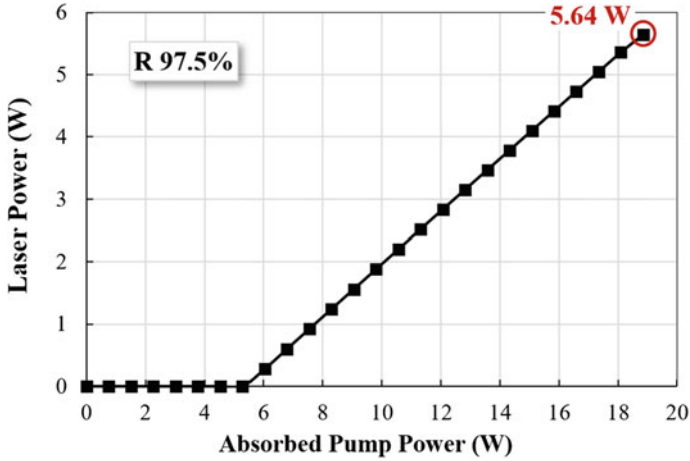


**Fig. 6.28** Absorbed pump-flux distributions along five transversal cross-sections (1, 2, 3, 4 and 5) of the three 2.5 mm diameter, 25 mm length Ce:Nd:YAG rods, obtained through Zemax<sup>®</sup> numerical analysis [20]



**Fig. 6.29** Schematic design of the laser resonator for multimode solar laser extraction from one of the three Ce:Nd:YAG rods [20]





**Fig. 6.30** Numerically calculated laser output power from one of the three Ce:Nd:YAG rods in LASCAD™ as a function of the absorbed solar power, for the output mirror reflectivity (R) of 97.5%

## References

1. Simpson, G.R.: Continuous sun-pumped room temperature glass laser operation. *Appl. Opt.* **3**(6), 783–784 (1964). <https://doi.org/10.1364/AO.3.000783>
2. Young, C.G.: A sun-pumped cw one-watt laser. *Appl. Opt.* **5**(6), 993–997 (1966). <https://doi.org/10.1364/AO.5.000993>
3. Arashi, H., Oka, Y., Sasahara, N., Kaimai, A., Ishigame, M.: A solar-pumped cw 18 W Nd:YAG laser. *Jpn. J. Appl. Phys.* **23**(Part 1, No. 8), 1051–1053 (1984). <https://doi.org/10.1143/jjap.23.1051>
4. Weksler, M., Shwartz, J.: Solar-pumped solid-state lasers. *IEEE J. Quantum Electron.* **24**(6), 1222–1228 (1988). <https://doi.org/10.1109/3.247>
5. Benmair, R.M.J., Kagan, J., Kalisky, Y., Noter, Y., Oron, M., Shimony, Y., Yogev, A.: Solar-pumped Er, Tm, Ho:YAG laser. *Opt. Lett.* **15**(1), 36–38 (1990). <https://doi.org/10.1364/OL.15.000036>
6. Krupkin, V., Kagan, J., Yogev, A.: Nonimaging optics and solar laser pumping at the Weizmann Institute, vol. 2016. SPIE's 1993 International Symposium on Optics, Imaging, and Instrumentation. SPIE, (1993). <https://doi.org/10.1117/12.161945>
7. Lando, M., Kagan, J., Linyekin, B., Dobrusin, V.: A solar-pumped Nd:YAG laser in the high collection efficiency regime. *Optics Communications* **222**(1), 371–381 (2003). [https://doi.org/10.1016/S0030-4018\(03\)01601-8](https://doi.org/10.1016/S0030-4018(03)01601-8)
8. Lando, M., Shimony, Y., Benmair, R.M.J., Abramovich, D., Krupkin, V., Yogev, A.: Visible solar-pumped lasers. *Opt. Mater.* **13**(1), 111–115 (1999). [https://doi.org/10.1016/S0925-3467\(99\)00019-1](https://doi.org/10.1016/S0925-3467(99)00019-1)
9. Yabe, T., Ohkubo, T., Uchida, S., Yoshida, K., Nakatsuka, M., Funatsu, T., Mabuti, A., Oyama, A., Nakagawa, K., Oishi, T., Daito, K., Behgol, B., Nakayama, Y., Yoshida, M., Motokoshi, S., Sato, Y., Baasandash, C.: High-efficiency and economical solar-energy-pumped laser with Fresnel lens and chromium codoped laser medium. *Appl. Phys. Lett.* **90**(26), 261120 (2007). <https://doi.org/10.1063/1.2753119>
10. Dinh, T.H., Ohkubo, T., Yabe, T., Kuboyama, H.: 120 watt continuous wave solar-pumped laser with a liquid light-guide lens and an Nd:YAG rod. *Opt. Lett.* **37**(13), 2670–2672 (2012). <https://doi.org/10.1364/OL.37.002670>

11. Dinh, T.H., Ohkubo, T., Yabe, T.: Development of solar concentrators for high-power solar-pumped lasers. **53**, 2711 (2014). <https://doi.org/10.1364/ao.53.002711>
12. Xu, P., Yang, S., Zhao, C., Guan, Z., Wang, H., Zhang, Y., Zhang, H., He, T.: High-efficiency solar-pumped laser with a grooved Nd:YAG rod. *Appl. Opt.* **53**(18), 3941–3944 (2014). <https://doi.org/10.1364/AO.53.003941>
13. Liang, D., Almeida, J.: Highly efficient solar-pumped Nd:YAG laser. *Opt. Express* **19**(27), 26399–26405 (2011). <https://doi.org/10.1364/OE.19.026399>
14. Guan, Z., Zhao, C., Li, J., He, D., Zhang, H.: 32.1 W/m<sup>2</sup> continuous wave solar-pumped laser with a bonding Nd:YAG/YAG rod and a Fresnel lens. *Opt. Laser Technol.* **107**, 158–161 (2018). <https://doi.org/10.1016/j.optlastec.2018.05.039>
15. Liang, D., Vistas, C.R., Almeida, J., Tiburcio, B.D., Garcia, D.: Side-pumped continuous-wave Nd:YAG solar laser with 5.4% slope efficiency. *Solar Energy Mater. Solar Cells* **192**, 147–153 (2019). <https://doi.org/10.1016/j.solmat.2018.12.029>
16. Vistas, C., Liang, D., Almeida, J., Tibúrcio, B., Garcia, D., Catela, M., Costa, H., Guillot, E.: Ce:Nd:YAG side-pumped solar laser. *J. Photonics Energy* **11**(1), 018001 (2021). <https://doi.org/10.1117/1.JPE.11.018001>
17. Liang, D., Almeida, J., Vistas, C.R., Guillot, E.: Solar-pumped Nd:YAG laser with 31.5W/m<sup>2</sup> multimode and 7.9W/m<sup>2</sup> TEM<sub>00</sub>-mode collection efficiencies. *Solar Energy Mater. Solar Cells* **159**, 435–439 (2017). <https://doi.org/10.1016/j.solmat.2016.09.048>
18. Liang, D., Almeida, J., Garcia, D., Tibúrcio, B.D., Guillot, E., Vistas, C.R.: Simultaneous solar laser emissions from three Nd:YAG rods within a single pump cavity. *Sol. Energy* **199**, 192–197 (2020). <https://doi.org/10.1016/j.solener.2020.02.027>
19. Garcia, D., Liang, D., Vistas, C.R., Costa, H., Catela, M., Tibúrcio, B.D., Almeida, J.: Ce:Nd:YAG Solar Laser with 4.5% solar-to-laser conversion efficiency. **15**(14), 5292 (2022). <https://doi.org/10.3390/en15145292>
20. Liang, D., Vistas, C.R., Garcia, D., Tibúrcio, B.D., Catela, M., Costa, H., Guillot, E., Almeida, J.: Most efficient simultaneous solar laser emissions from three Ce:Nd:YAG rods within a single pump cavity. *Sol. Energy Mater. Sol. Cells* **246**, 111921 (2022). <https://doi.org/10.1016/j.solmat.2022.111921>
21. Liang, D., Vistas, C.R., Tibúrcio, B.D., Almeida, J.: Solar-pumped Cr:Nd:YAG ceramic laser with 6.7% slope efficiency. *Solar Energy Mater. Solar Cells* **185**, 75–79 (2018). <https://doi.org/10.1016/j.solmat.2018.05.020>
22. Vistas, C.R., Liang, D., Garcia, D., Almeida, J., Tibúrcio, B.D., Guillot, E.: Ce:Nd:YAG continuous-wave solar-pumped laser. *Optik* **207**, 163795 (2020). <https://doi.org/10.1016/j.ijleo.2019.163795>
23. Almeida, J., Liang, D., Guillot, E.: Improvement in solar-pumped Nd:YAG laser beam brightness. *Opt. Laser Technol.* **44**(7), 2115–2119 (2012). <https://doi.org/10.1016/j.optlastec.2012.03.017>
24. Almeida, J., Liang, D., Garcia, D., Tibúrcio, B.D., Costa, H., Catela, M., Guillot, E., Vistas, C.R.: 40 W Continuous wave Ce:Nd:YAG solar laser through a fused silica light guide. **15**(11), 3998 (2022). <https://doi.org/10.3390/en15113998>
25. Kalogirou, S.A.: Solar thermal collectors and applications. *Prog. Energy Combust. Sci.* **30**(3), 231–295 (2004). <https://doi.org/10.1016/j.pecs.2004.02.001>
26. Mousazadeh, H., Keyhani, A., Javadi, A., Mobli, H., Abrinia, K., Sharifi, A.: A review of principle and sun-tracking methods for maximizing solar systems output. *Renew. Sustain. Energy Rev.* **13**(8), 1800–1818 (2009). <https://doi.org/10.1016/j.rser.2009.01.022>
27. Reddy, D.S., Khan, M.K.: Stationary point focus solar concentrators—a review. **46**(5), 5678–5702 (2022). <https://doi.org/10.1002/er.7612>
28. Bouzakri, H., Abbou, A., Tijani, K., Abousserhane, Z.: Biaxial equatorial solar tracker with high precision and low consumption: modelling and realization. *Int. J. Photoenergy* **2021**, 6679576 (2021). <https://doi.org/10.1155/2021/6679576>
29. Chang, C.: 5—Tracking solar collection technologies for solar heating and cooling systems. In: Wang, R.Z., Ge, T.S. (eds.) *Advances in Solar Heating and Cooling*, pp. 81–93. Woodhead Publishing, (2016). <https://doi.org/10.1016/B978-0-08-100301-5.00005-9>

30. Grigoriev, V., Milidonis, K., Blanco, M.: Sun tracking by heliostats with arbitrary orientation of primary and secondary axes. *Sol. Energy* **207**, 1384–1389 (2020). <https://doi.org/10.1016/j.solener.2020.07.086>
31. Lando, M., Kagan, J., Linyekin, B., Sverdalov, L., Pecheny, G., Achiam, Y.: An astigmatic corrected target-aligned solar concentrator. *Opt. Commun.* **180**(1), 127–132 (2000). [https://doi.org/10.1016/S0030-4018\(00\)00686-6](https://doi.org/10.1016/S0030-4018(00)00686-6)
32. The Canadian Institute for the Energies and Applied Research. <https://wis-wander.weizmann.ac.il/content/harnessing-sun> (1997)
33. Arashi, H., Cooke, D., Naito, H.: Fivefold increase in solar laser output with a nonimaging concentrator. *Jpn. J. Appl. Phys.*, **34**(Part 1, No. 9A), 4795–4798 (1995). <https://doi.org/10.1143/jjap.34.4795>
34. Levitan, R., Rosin, H., Levy, M.: Chemical reactions in a solar furnace—direct heating of the reactor in a tubular receiver. *Sol. Energy* **42**(3), 267–272 (1989). [https://doi.org/10.1016/0038-092X\(89\)90017-0](https://doi.org/10.1016/0038-092X(89)90017-0)
35. Epstein, M., Vishnevetsky, I., Segal, A., Rubin, R., Lieberman, D.: Research and development in the solar research facilities unit of the weizmann institute of science: past, present, and future. *The Int. J. Environ. Sustain.* **9**, 97–116 (2014). <https://doi.org/10.18848/2325-1077/CGRP/v09i04/55113>
36. Solar furnaces and concentrating solar systems. <https://www.promes.cnrs.fr/en/infrastructure-solaire/moyens-solaires/solar-furnaces-and-concentrating-solar-systems/> (2022)
37. Johnson, S.C.: Solar pumping converts broadband sunlight into efficient laser light. In: *Laser Focus World: Lasers and Sources*. (2022). <https://www.laserfocusworld.com/lasers-sources/article/14283698/solar-pumping-converts-broadband-sunlight-into-efficient-laser-light>
38. Aieta, F., Genevet, P., Kats, M., Capasso, F.: Aberrations of flat lenses and aplanatic metasurfaces. *Opt. Express* **21**(25), 31530–31539 (2013). <https://doi.org/10.1364/OE.21.031530>
39. Rocha, M.C., Goncharov, A.V.: Aplanatic meniscus lens corrector for Ritchey-Chrétien telescopes. *Opt. Express* **30**(4), 6076–6089 (2022). <https://doi.org/10.1364/OE.450473>
40. Pernechele, C.: Hyper hemispheric lens. *Opt. Express* **24**(5), 5014–5019 (2016). <https://doi.org/10.1364/OE.24.005014>
41. Heraeus: Properties of fused silica. [https://www.heraeus.com/en/hca/fused\\_silica\\_quartz\\_kno\\_wledge\\_base\\_1/properties\\_1/properties\\_hca.html](https://www.heraeus.com/en/hca/fused_silica_quartz_kno_wledge_base_1/properties_1/properties_hca.html) (2022)
42. Koechner, W.: *Solid-State Laser Engineering*. Springer (2006). <https://doi.org/10.1007/0-387-29338-8>
43. Clarkson, W.A.: Thermal effects and their mitigation in end-pumped solid-state lasers. *J. Phys. D Appl. Phys.* **34**(16), 2381–2395 (2001). <https://doi.org/10.1088/0022-3727/34/16/302>
44. Winston, R., Minano, J.C., Benitez, P.G.: *Nonimaging Optics*. Elsevier (2005). <https://doi.org/10.1016/B978-0-12-759751-5.X5000-3>
45. Winston, R.: Principles of solar concentrators of a novel design. *Sol. Energy* **16**(2), 89–95 (1974). [https://doi.org/10.1016/0038-092X\(74\)90004-8](https://doi.org/10.1016/0038-092X(74)90004-8)
46. Welford, W.T.: *High Collection Nonimaging Optics*. Elsevier, (1989). <https://doi.org/10.1016/B978-0-12-742885-7.X5001-3>
47. Rabl, A., Goodman, N.B., Winston, R.: Practical design considerations for CPC solar collectors. *Sol. Energy* **22**(4), 373–381 (1979). [https://doi.org/10.1016/0038-092X\(79\)90192-0](https://doi.org/10.1016/0038-092X(79)90192-0)
48. McIntire, W.R.: Truncation of nonimaging cusp concentrators. *Sol. Energy* **23**(4), 351–355 (1979). [https://doi.org/10.1016/0038-092X\(79\)90130-0](https://doi.org/10.1016/0038-092X(79)90130-0)
49. Ning, X., O’Gallagher, J., Winston, R.: Optics of two-stage photovoltaic concentrators with dielectric second stages. *Appl. Opt.* **26**(7), 1207–1212 (1987). <https://doi.org/10.1364/AO.26.001207>
50. Ning, X., Winston, R., O’Gallagher, J.: Dielectric totally internally reflecting concentrators. *Appl. Opt.* **26**(2), 300–305 (1987). <https://doi.org/10.1364/AO.26.000300>
51. ASTM Standard G173–03 (2020), Standard Tables for Reference Solar Spectral Irradiances: Direct Normal, and Hemispherical on 37° Tilted Surface (2020). <https://doi.org/10.1520/G0173-03R20>

52. Prah1, S.: Nd:YAG—Nd:Y<sub>3</sub>Al<sub>5</sub>O<sub>12</sub>. <https://omlc.org/spectra/lasermedia/html/052.html> (2017)
53. Rapaport, A., Zhao, S., Xiao, G., Howard, A., Bass, M.: Temperature dependence of the 1.06- $\mu$ m stimulated emission cross section of neodymium in YAG and in GSGG. *Appl. Opt.* **41**(33), 7052–7057 (2002). <https://doi.org/10.1364/AO.41.007052>
54. Tai, Y., Zheng, G., Wang, H., Bai, J.: Near-infrared quantum cutting of Ce<sup>3+</sup>–Nd<sup>3+</sup> co-doped Y<sub>3</sub>Al<sub>5</sub>O<sub>12</sub> crystal for crystalline silicon solar cells. *J. Photochem. Photobiol., A* **303–304**, 80–85 (2015). <https://doi.org/10.1016/j.jphotochem.2015.02.009>